MNRAS **000**, 1–19 (2011) Preprint 6 February 2020 Compiled using MNRAS LATEX style file v3.0

TESS observations of Be stars: a new interpretation

L. A. Balona[1⋆] and D. Ozuyar[2]
[1] *South African Astronomical Observatory, P.O. Box 9, Observatory 7935, South Africa*
[2] *Ankara University, Faculty of Science, Dept. of Astronomy and Space Sciences, 06100, Tandogan, Ankara, Turkey*

Accepted .... Received ...

ABSTRACT
Light curves of 57 classical Be stars in *TESS* sectors 1–15 are examined. In most Be stars, the periodogram shows groups at a fundamental and one or more harmonics, which we attribute to rotation. In about 40 percent of the stars, the group is just a single narrow or slightly broadened peak. In about 30 percent, it consists of a multiple, closely spaced peaks. These groups can be interpreted as non-coherent variations most likely associated with photospheric gas clouds. Approximate rotational frequencies for about 74 percent of the stars can be derived. Comparison with the projected rotational velocities shows that the photometric frequency is consistent with rotation. The first harmonic plays a prominent role in many Be stars and manifests itself in either single-wave or double-wave light curves. The reduction in amplitude of β Cep pulsations in a few Be stars during an outburst and their subsequent recovery is most likely an obscuration effect. Other instances of possible obscuration of the photosphere are suspected. A simple model, which attempts to explain these observations and other general properties of Be stars, is proposed.

Key words: stars: emission-line, Be – stars: rotation – stars: oscillations

1 INTRODUCTION

The classical Be stars are dwarf and giant B stars that show, or have shown at some time, emission in the core of some Balmer lines (particularly the Hα line) (Slettebak 1979; Porter & Rivinius 2003). Stars in which the emission is a result of binary interaction are excluded from the definition. Pre-main sequence stars are also excluded. The emission is thought to be a result of mass loss from the star which is greatly assisted by rapid rotation.

In many Be stars, spectroscopic line profile and light variations characteristic of non-radial pulsation (NRP) are observed with periods of about one day. For this reason it is generally believed that NRP acts as the trigger for mass-loss outbursts which occur from time to time (Rivinius 2013). Because the additional velocity provided by NRP is relatively small, this mechanism requires the star to be rotating in excess of about 90 percent of the critical rotational velocity at the equator. In this hypothesis, every Be star must be rotating very near critical velocity (Townsend et al. 2004).

However, it has been shown that, as a group, Be stars rotate at rates which are well below the critical rotation rate. Cranmer (2005) found that early-type Be stars have an approximately uniform spread of intrinsic rotation speed that extends from 0.4–0.6 of critical, though a few may be rotating near critical velocity. Late-type Be stars exhibit progressively narrower ranges of rotation speed as the effective temperature decreases. The lower limit rises to reach critical rotation for the coolest Be stars. More recently, Zorec et al. (2016) arrived at the same conclusion. They found that in most Be stars the ratio of equatorial rotational velocity relative to the critical rotational velocity is $v/v_c \approx 0.65$. This ratio is characterized by a wide range $0.3 < v/v_c < 0.95$, suggesting that the probability that all Be stars are critical rotators is extremely low (see also Cochetti et al. 2019).

In this paper we take the view that NRP, if present, is incidental and cannot play the main role in the mass loss mechanism. An alternative mechanism needs to be found.

It is generally accepted that early-type stars have radiative envelopes which cannot sustain magnetic fields. Therefore photospheric activity cannot exist. This has always been an important motivation for NRP as the source of mass loss in Be stars. However, recent space photometry shows that a significant fraction of A and B stars have periods which are indistinguishable from the rotational periods (Balona 2013, 2016, 2017). A recent study concludes that about 35 percent of all mid- to late-B stars exhibit rotational modulation (Balona 2019).

It therefore appears that starspots may be present in many early-type stars. We may presume starspots are sources of activity. Such activity occurs through the presence of a localized magnetic field and magnetic reconnection, leading to flares and ejection of material, as in the Sun. This

⋆ E-mail: lab@saao.ac.za

idea is the basis for the mechanism first proposed by Balona (2003) and discussed in this paper.

The quasi-periodicity of many Be stars tends to cluster in two frequency groups, one twice the frequency of the other. An example of this tendency can be found in ground-based photometry of several Be stars in the open cluster NGC 3766 (Balona et al. 1991). In some seasons the fundamental group dominates and the light curve is a single wave. At other seasons the first harmonic group dominates and the light curve has a double-wave form. Photometric observations from space have confirmed this general pattern. Examples from the *MOST* satellite include HD 163868 (Walker et al. 2005), HD 127756 and HD 217543 (Cameron et al. 2008). There are several examples from *CoRoT* as well (Neiner et al. 2009; Semaan et al. 2018). The same is found in 48 Lib observed by the *STEREO* satellite (Ozuyar et al. 2018) as do two of the three Be stars observed by *Kepler* (Rivinius et al. 2016b). These frequency groups have been interpreted as due to a large number of g-modes driven by the κ opacity mechanism. They can perhaps also be regarded as incoherent variations leading to quasi-periodicity. This behaviour is a very important clue to the nature of mass loss and short-period variability and is included in the new hypothesis discussed below.

In this paper we present photometric *TESS* observations of classical Be stars observed in Sectors 1–15. Observations of the most interesting stars and stars with the longest time series are presented in the main body of the text. Discussion of the remaining stars is deferred to an Appendix. A major objective is to investigate the morphology of the light curves in order to provide clues to the mass-loss mechanism. Where it is possible, we attribute the frequencies or frequency groups to rotational modulation. Our aim is to test this idea by comparing the projected rotational velocity, $v \sin i$, with the equatorial rotational velocity, v, derived from the photometric frequency and the stellar radius. For this purpose we obtain stellar radius estimates using the luminosity derived from the *GAIA* DR2 parallax (Gaia Collaboration et al. 2016, 2018) and the effective temperature. Before describing the *TESS* observations, we discuss a new model for the mass-loss mechanism.

2 THE MASS-LOSS MECHANISM

We know that rotational modulation of the light curve appears to occur in a large fraction of B stars (Balona 2019) and may even be present in O stars (Ramiaramanantsoa et al. 2014, 2018). This indicates the possible presence of a starspot or group of spots which, in turn, suggests the presence of localized magnetic fields.

The idea that early B stars may have sub-surface convective zones was postulated by Cantiello et al. (2009) and further discussed by Cantiello & Braithwaite (2011). They propose a convection zone close to the stellar surface, caused by a peak in the opacity associated with iron-group elements. Dynamo action in this zone is expected to generate surface magnetic fields of around 5–300 G, resulting in bright magnetic spots of size comparable to the local pressure scale height.

Observations of A stars also indicate the presence of rotational modulation (Balona 2013, 2017). In this case, surface magnetic spots might be caused by the presence of small envelope convective layers at or just below the stellar surface due to recombination of H and He (Cantiello & Braithwaite 2019). The occurrence and detectability of this type of spot decrease moving from A to late B-type stars. Cantiello & Braithwaite (2019) predicts regions of the H–R diagram where subsurface convection is unlikely to have any effect, and weak magnetic fields and photometric variability due to magnetic spots should be absent/undetectable in the majority of non-Ap/Bp stars. However, observations show that rotational modulation seems to be present in early-A and late B stars as well (Balona 2017, 2019; Sikora et al. 2019).

The most likely explanation for the observed rotational modulation in B stars is the presence of thermal spots resulting from small-scale magnetic fields. This, in turn, means that magnetic reconnection and flaring may be possible. Flares on B stars would be difficult to detect, though one or two late B stars are known to flare (Balona 2013). It cannot be proved that the flare originates on the B stars, though the very high energies rule out flaring on a cool companion. There have been a number of reports of transient features in Be stars with typical lifetimes of an hour (see Porter & Rivinius 2003), though at present there is no evidence that these are related to magnetic reconnection. In addition, there is a group of active Be stars, the γ Cas variables, which are X-ray emitters (Smith et al. 2016). The origin of the X-rays is still not known. Generation of X-rays by accretion to a white dwarf does not seem to fit the data. Whether or not magnetic flares can account for the observations has not been considered.

About 10 percent of mid- to early-B main sequence stars have strong dipole magnetic fields, presumed to be of fossil origin (Grunhut et al. 2017). Weaker fields may be present, but difficult to measure. For example, Kholtygin et al. (2017) conclude that among early-type stars, magnetic field strengths obey a log-normal law. Hubrig et al. (2017) observed the well-known Be star λ Eri and conclude that a global field might be present, though the result is inconclusive. In short, the presence of magnetic fields in Be stars is highly controversial and still under debate. It has been shown that a global field strength of just 10 G can significantly disrupt the disc in a Be star, while a field of 100 G completely destroys the disc in just a few days (ud-Doula et al. 2018). If such a global field is present it is likely to be no more than a few Gauss and not detectable with current techniques. This is, however, sufficient to control the dynamics of ionized parcels of gas, as we know from the Sun which has a global dipolar field of the order of about 1 G.

The observational and theoretical background described above allows for a model of mass loss in Be stars which does not require the stars to be rotating near critical velocity. It is proposed that the mass ejection is a result of energy release from magnetic reconnection associated with localized magnetic fields generated by sub-surface convection. A sudden energy release describes a Be outburst quite well.

A very important clue to the mass-loss mechanism is the fact that two frequency groups, one twice the frequency of the other, are commonly present in Be star light curves, as already mentioned. Further examples of this phenomenon will be illustrated below. The new mechanism must there-

fore include a way in which such frequency groups arise in a natural way. A weak dipole magnetic field which is tilted relative to the rotational axis may be one way in which the rotational harmonic is generated. The magnetic equator intersects the geographic equator in two diametrically opposite points. Matter ejected by a magnetic reconnection event will be highly ionized and will move along closed magnetic field lines, trapped in a torus tilted with respect to the equator. Rapid rotation will tend to concentrate material at the two diametrically opposite points where centrifugal acceleration is the highest. This could possibly generate a double-wave light curve or a single-wave light curve depending on the amount of gas trapped in each of the two points.

Our proposal is that a magnetic reconnection or flaring event at any point on the stellar surface will tend to feed matter into one or both of these locations leading to quasi-periodic rotational modulation which could persist for months. In this scenario it is not only the spot or spots which might cause rotational modulation, but also the gas trapped at the two diametrically opposite points. The fundamental frequency in both cases will be the rotational frequency, or perhaps a narrow range of frequencies if differential rotation is present. One does not expect coherence not only because multiple close frequencies may be involved, but also because the amount of trapped gas will be constantly changing as will be the location and size of the spot or spots.

A light curve with a quasi-period similar to the rotation period in one season and with a period which is half as long in another season can thus arise. In other words, this might be a possible explanation for the common occurrence of two frequency groups in which the relative amplitudes change with time.

It is expected that matter will be slowly released from the trapping points and will also escape along open field lines. It will be dragged and accelerated by the rapid rotation of the star. Depending on the rotational velocity, the gas will reach circular orbital speeds at some distance from the star if it is still ionized. After some time the gas, predominantly H and He, will cool, become neutral (and thus unaffected by the magnetic field) and slowly dissipate into the inner circumstellar disk, rotating at Keplerian velocity.

In this model, whether a circumstellar disk is formed or not depends on the presence of a tilted dipole magnetic field and sufficiently rapid rotation to reach circular velocity while the gas is still ionized. Mass ejection is more likely to occur in a rapid rotator, but since large ejection velocities are expected in magnetic reconnection, mass loss can still occur if the star is well below the critical rotation rate. This is in line with the broad range of rotational velocities in Be stars found by Cranmer (2005) and Zorec et al. (2016).

In the intense radiation field of an early B star, matter will remain ionized to large distances. Even if the star is rotating well below critical velocity, the long lever arm provided by the magnetic field will ensure that the ejected matter attains circular velocity while still ionized and under control of the magnetic field.

On the other hand, the weak radiation field in a late Be star limits the ionization radius closer to the photosphere. The lever arm is therefore shorter and requires a star already rotating closer to critical for the gas to reach circular velocity while still ionized. This might explain why late Be stars are rotating in a narrow band close to the critical rotation speed as found by Cranmer (2005) and Zorec et al. (2016).

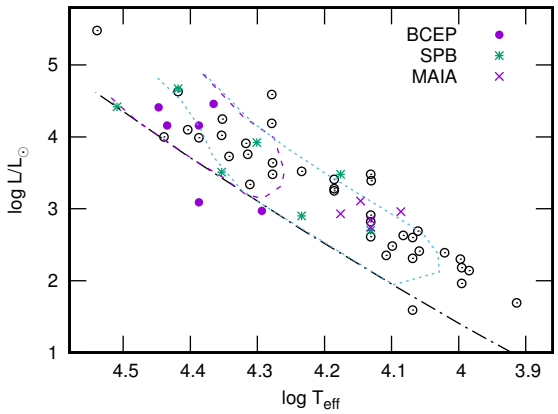

Figure 1. The H-R diagram showing the Be stars observed by *TESS*. Be stars which are also β Cep (BCEP), SPB or Maia pulsators are indicated. Also shown is the theoretical zero-age main sequence (dash-dotted line), the instability regions of the β Cep (dashed line) and SPB (dotted line) pulsating stars.

It is evident that the condition to attain circular velocity occurs in a far larger range of rotational velocities in early-type stars compared to late-type stars. This might explain why most Be stars are of early type. Since the co-rotating ionized region is much larger in early B stars, it follows that activity will be higher in these stars. In this way one can also understand why early Be stars are more active than late Be stars.

The model described above bears some similarity to the rigidly rotating magnetosphere model of Townsend & Owocki (2005). In this model, a strong tilted dipole magnetic field is assumed (whereas our model supposes a weak field) with mass loss driven by a stellar wind (whereas our model assumes, in addition, a flare-like eruption). Magnetic confinement of line-driven wind outflows has been studied by ud-Doula & Owocki (2002) and Ud-Doula et al. (2008, 2009). However, the context of these calculations is not the same as in our model and does not include material ejected by a flaring outburst. Owocki (2004) briefly discusses mass ejection by surface explosions or magnetic flares.

The sketch presented above and first postulated by Balona (2003) is only a working model. There is clearly a need for in-depth theoretical study as well as observations targeted at disproving or modifying the model. In any case, the notion of quiescent B-star radiative atmospheres is no longer tenable and requires a change in long-held assumptions.

3 THE *TESS* DATA

The *TESS* satellite obtains precise wide-band photometry for thousands of stars with two-minute cadence in a given sector of the sky. There are 26 partially overlapping sectors and each sector is observed for approximately one month. The light curves are obtained using pre-search data conditioning (PDC) which corrects for time-correlated instrumen-

Table 1. List of Be stars selected for analysis. The *TESS* catalogue number, TIC, and the HD number are listed. This is followed by the variability classification based purely on the *TESS* light curve. The number of *TESS* sectors is given by N. The V magnitude, the effective temperature, $T_{\rm eff}$ (K), and the literature reference for $T_{\rm eff}$ are given. The stellar luminosity determined from the *GAIA* parallax is shown and is followed by the adopted rotational frequency $\nu_{\rm rot}$ (d^{-1}), the derived equatorial rotational velocity, v ($\mathrm{km\,s^{-1}}$) and the projected rotational velocity, $v\sin i$ ($\mathrm{km\,s^{-1}}$). The last column gives the spectral classification.

TIC	HD	Var Type	N	V	$T_{\rm eff}$	Ref	$\log\frac{L}{L_\odot}$	$\nu_{\rm rot}$	v	$v\sin i$	Sp Type
23037766	57150	ROT	1	4.670	22000	2	3.73	1.07	270	210	B2V + B3IVne
42360166	191610	ROT	2	4.930	20470	9	3.34	1.5	280	320	B2.5III
47296054	214748	ROT	1	4.180	11500	2	2.69	0.836	240	180	B8/9IV/V
52665242	47054	ROT	1	5.520	13520	1	2.91	1.145	300	260	B8IV/Ve shell
53992511	209522	SPB+ROT	1	5.952	22570	1	3.51	1.6	300	280	B3V + B:
55295028	33599	ROT+BCEP	13	8.970	23200	7	4.46	0.905	480	200	B3p shell
56179720	30076	SPB	1	5.810	26190	1	4.67	-	-	180	B1V?e
65803653	56014	BCEP+ROT	1	4.650	24380	1	4.16	1.3	440	210	B2V(e) shell
67251066	198183	ROT	1	4.540	15330	1	3.25	1.1	330	120	B7.5IV
71132174	28497	SPB+ROT	1	5.410	32310	9	4.42	1.4	370	230	B1Ve
71727949	41335	-	1	5.210	22500	2	4.25	-	-	340	B1:IV/V:nne shell
75047606	79621	ROT	2	5.920	11710	1	2.31	1.67	290	170	B9V
81584371	54309	ROT	1	5.830	26190	1	4.63	0.75	380	200	B1.5III
99115271	193911	ROT	1	5.560	15330	1	3.41	0.529	190	200	B7IV/Ve shell
120967488	178475	ROT	1	5.249	18950	1	3.48	1.0	260	230	B5/8
139385056	58978	BCEP	1	5.560	28000	1	4.41	-	-	280	B0.5IVn(e)p
139472176	14850	ROT	1	8.400	13500	7	3.39	0.773	350	200	B7III/IVe
140214221	37795	ROT	2	2.652	12200	2		1.841		180	B7IVe
144028101	135734	MAIA	1	4.274	13520	1		-		279	B8Ve
148316007	49319	BCEP+ROT	2	6.625	24380	1	3.09	2.5	400	245	B2/3IVne
148917425	109387	MAIA+ROT	2	3.890	14000	6	3.11	0.882	270	200	B6III(n)
151300497	155806	-	1	5.530	34600	1	5.48	-		115	O7.5V((f))z(e)
159117671	112028	ROT+ROT	1	5.350	9650	1	2.14	1.252	270	200	A1IIIp shell
174664153	61925	ROT	2	6.004	22570	1	4.02	1.019	350	200	B3IV(e);
175523591	63215	ROT	2	5.870	17140	1	2.90	2.5	400	271	B6Vnn
195744427	199629	ROT	1	3.940	9900	1	1.96	-		219	A0.5IIIn
207176480	19818	ROT+FLARE	2	9.060	11710	1	1.59	0.298	90		B9/A0Vne:
230981971	10144	ROT	1	0.460	15000	8	3.48	0.75	350	260	B4V(e)
234230792	49330	BCEP+ROT	1	8.950	27200	7	4.16	1.47	400	200	B0:nnep
245286665	192044	ROT	1	5.920	15330	1	3.28	1.039	330	280	B7IV/V:ne shell
258704817	129954	-	1	5.880	24380	1	3.99	-	-	180	B2.5V
259449942	60855	ROT	1	5.700	20760	1	3.91	1.1	390	230	B4III:n shell
260640910	46860	SPB+ROT	12	5.707	13520	1	2.70	1.392	290	200	B8III
270219259	209014	MAIA	1	5.620	12200	1	2.96	-	-	350	B8III shell
277103567	37935	ROT	3	6.281	9940	5	2.30	1.497	360	209	B9.5V
279430029	53048	ROT	13	7.920	18950	1	3.64	1.784	550		B5/7Vn(e:)
281741629	CD-56 152	-	1	10.180	19000	4	4.59	-	-	180	sdB?/Be?
296969980	131492	SPB	1	5.110	20000	2	3.92	-	-	100	B2IV/V
302962039	78764	-	4	4.654	19000	2	4.19	-		140	B2IV:n(e) He-s
308748912	68423	-	6	6.313	12100	2	2.63	-	-	26	B7IVek;
334776134	91120	ROT	1	5.580	11453	10	2.41	1.3	270	250	B9IV/V shell
341040849	64831	ROT	4	7.830	13520	1	2.61	1.406	260		B8Vn(e)
355653322	224686	ROT	1	4.470	10500	2	2.39	1.266	300	275	B9IIIn
358467471	65663	-	5	6.741	13520	1	3.48	-		120	B8IIIe
363748801	149671	ROT	1	5.882	13520	1	2.82	1.555	370	230	B8:V:
364398342	66194	ROT	7	5.810	20632	3	3.76	1.25	380	200	B2IVn(e)p(Si)
405520863	110335	ROT	1	4.940	17140	1	3.52	1.298	430	244	B6IVe
408382023	83953	MAIA+ROT	1	4.760	15000	2	2.93	1.55	340	260	B6V(e)
409358619	124367	BCEP+ROT	1	5.070	19650	2	2.97	2.768	370	280	B5:Vnne
423528378	107348	ROT	1	5.210	12830	2	2.35	2.306	350	250	B8Vn
425224332	58715	ROT	1	2.890	12560	11	2.48	1.61	300	260	B8IV/Ve shell
427395049	37041	-	1	6.390	27500	2	4.00	-	-	130	O9.5Vpe
439397894	225132	ROT	1	4.543	9900	1	2.18	1.441	300	211	A0:IV
443616529	98058	DSCT	1	4.467	8200	2	1.69	-		230	A7IV shell
452163402	100673	ROT	1	4.614	11710	1	2.60	1.364	330	125	B9V(e?)
463103957	88661	ROT	2	5.750	25350	9	4.10	1.36	400	220	B2IVnep
469421586	195554	MAIA+ROT	1	5.889	13520	1	2.85	1.66	400	240	B8IV/V

References to $T_{\rm eff}$:
1 - MK Type (Pecaut & Mamajek 2013); 2 - Arcos et al. (2018); 3 - Silaj & Landstreet (2014); 4 - Silva & Napiwotzki (2011); 5 - Balona (1994); 6 - Saad et al. (2004); 7 - Levenhagen & Leister (2006); 8 - Domiciano de Souza et al. (2014); 9 - Zorec et al. (2016); 10 - Shokry et al. (2018); 11 - Harmanec et al. (2019).

Table 2. List of sectors and total timespan, Δt in days for each star.

TIC	Sectors	Δt	TIC	Sectors	Δt
23037766	7	24.5	245286665	14	26.9
42360166	14,15	54.1	258704817	12	27.9
47296054	2	27.4	259449942	7	24.5
52665242	6	21.8	260640910	1–6,8–13	357.1
53992511	1	27.9	270219259	1	27.9
55295028	1– 13	357.1	277103567	2,4,5	110.2
56179720	5	26.3	279430029	1–13	357.1
65803653	7	24.5	281741629	2	27.4
67251066	15	26.0	296969980	12	27.9
71132174	5	26.3	302962039	9–12	108.0
71727949	6	21.8	308748912	1,4,8–11	298.6
75047606	8,9	51.1	334776134	9	23.6
81584371	7	24.5	341040849	4,7–9	157.6
99115271	14	26.9	355653322	1	27.9
120967488	14	26.9	358467471	4,7–10	184.8
139385056	7	24.5	363748801	12	27.9
139472176	3	20.3	364398342	1,4,7–11	298.6
140214221	5,6	52.1	405520863	11	25.5
144028101	12	27.9	408382023	8	24.6
148316007	6,7	47.8	409358619	11	25.5
148917425	14,15	54.1	423528378	10	24.6
151300497	12	27.9	425224332	7	24.5
159117671	14	26.9	427395049	6	21.8
174664153	7,8	50.4	439397894	2	27.4
175523591	7,8	50.4	443616529	9	23.6
195744427	15	26.0	452163402	10	24.6
207176480	2,3	52.1	463103957	9,10	50.8
230981971	2	27.4	469421586	15	26.0
234230792	6	21.8			

tal signatures in the light curves (Jenkins et al. 2016). Each *TESS* pixel is 21 arcsec in size which is similar to the typical aperture size used in ground-based photoelectric photometry. The chance of contamination by a star of similar brightness is not negligible. However, for the stars discussed here, which are in any case mostly brighter than 8-th magnitude, there is no other object within the pixel of comparable brightness.

The stars selected for analysis were chosen from the BESS database of classical Be stars (Neiner et al. 2011). We decided to select the best-known Be stars from this list which have been observed in sectors 1–15 and to complement this number with a random selection of additional stars. In this way we obtained 57 stars which can be described in relative detail. It is our intention to present a complete analysis of all classical Be stars when all 26 sectors have been observed. The selected stars are listed in Table 1. The sectors observed and the total timespan for each star is given in Table 2.

The effective temperatures, $T_{\rm eff}$, of Be stars are poorly known because the line blanketing caused by circumstellar material leads to unreliable estimates from multicolour photometry. For this reason the value of $T_{\rm eff}$ was derived from spectroscopic modelling whenever possible. Failing this, it is estimated from the spectral type and luminosity class using the Pecaut & Mamajek (2013) calibration. The error in $T_{\rm eff}$, as estimated from the dispersion in spectral types, is about 1000 K. The spectral types are from the compilation by Skiff (2014).

Stellar luminosities were derived from *GAIA* DR2 parallaxes (Gaia Collaboration et al. 2016, 2018). The bolometric correction was obtained from $T_{\rm eff}$ using the Pecaut & Mamajek (2013) calibration. The reddening correction was derived from a three-dimensional reddening map by Gontcharov (2017). The formal error in luminosity, $\log L/L_\odot$, as estimated from the error in the parallax, bolometric correction and extinction, is about 0.05 dex, but is likely to be larger. The theoretical H–R diagram is shown in Fig. 1.

The projected rotational velocities in Table 1 are mostly from the catalogue of Głębocki & Gnaciński (2005) supplemented by more recent measurements when available. The typical error in $v \sin i$ for B stars can be estimated from the catalogue. The error increases with $v \sin i$ and ranges up to 60 km s^{-1}. A representative value of $\sigma_{v \sin i} = 30$ km s^{-1} is assumed. From the error in $\log L/L_\odot$ and $T_{\rm eff}$ it is easy to calculate the error in the derived stellar radius and hence the equatorial rotational velocity, v, deduced from the photometric rotational frequency, $\nu_{\rm rot}$. This error depends almost entirely on the error in $T_{\rm eff}$. The contribution from the luminosity error is small while the contribution from the error in $\nu_{\rm rot}$ is negligible. The typical value for the error in the derived equatorial rotational velocity is $\sigma_v \approx 40$ km s^{-1}.

3.1 Photometric Data and Analysis

To detect periodic stellar signals, the Lomb-Scargle (Lomb 1976; Scargle 1982) technique is used. However, the power spectrum does not provide information related to changes of frequency and amplitude with time. Such information may be very important in diagnosing the source of the variation and are best represented by a time-frequency diagram (Boashash 2015).

In obtaining the time-frequency diagram, the Lomb-Scargle periodogram was calculated in a fixed time window which was chosen to be five days as a compromise between good signal-to-noise ratio and reasonable frequency resolution. The window is shifted with a time step of 0.5 d. At each time step, the periodogram (amplitude vs frequency) is plotted. In the resulting time-frequency diagram, the amplitude is coded by color (or grey level in the printed version). The color or grey level is normalized to the highest amplitude in the periodogram.

4 VARIABILITY CLASSIFICATION

In the *General Catalogue of Variable Stars* (GCVS, Samus et al. 2017), the variability type BE is used for Be stars with mild to moderate light outbursts. The GCAS (γ Cas) type is used for eruptive early Be stars where outbursts may exceed 1 mag. These variations refer to the effects of the outburst itself and to circumstellar material on the light curve. There is no GCVS classification for hot rotational variables other than those with chemical peculiarities. For this reason, the ROT class was introduced. For a brief discussion on classification of variable stars see Balona et al. (2019).

While starspots may be present in Be stars, and may be detected in the light curve, circumstellar material is an important contribution to the light variation. The tentative framework that we adopt in describing the quasi-periodic

light variations in Be stars is that these are a result of co-rotating gas clouds ejected by active regions associated with starspots, rather than the starspots themselves. Starspots in B stars seem to be reasonably coherent over a month or two (Balona 2019). Co-rotating gas clouds may have much shorter lifetimes. They therefore could give rise to incoherent light variations with a quasi-period close to the rotation period of the star. In the periodogram this manifests as groups of peaks or broad humps of power at the approximate rotational frequency and its harmonic.

The Be stars lie in either, or both, the β Cep or SPB instability strips and it is likely that pulsations may be present. Some stars have high frequencies, but are too cool to be classified as β Cep and too hot for δ Scuti. These are classified as Maia variables (Balona et al. 2016). It is more difficult to distinguish SPB pulsations from rotation modulation as the frequency range overlaps. The criterion used in that if harmonics are present then rotation cannot be excluded and the ROT class is applied. From the fundamental photometric frequency, the equatorial rotational velocity is estimated. This will be compared with $v \sin i$ as a consistency test.

5 RESULTS

There are several stars where *TESS* observations cover many sectors. These are of particular interest as it allows exploration of how the star behaves over a period of many months. Certain well-observed stars are also of interest even if the observations are only from one sector. These stars are discussed below. The remaining stars, nearly all of which were observed in only one sector, are discussed in the Appendix. Some stars will be re-observed in future *TESS* sectors which, of course, may modify the results presented here.

5.1 TIC 42360166, 28 Cyg

Spectroscopic observations of 28 Cyg have generally confirmed the presence of a group of frequencies at around $1.56\,\mathrm{d}^{-1}$ (Peters & Penrod 1988; Pavlovski & Ruzic 1990; Hahula & Gies 1994) and also around $1.4\,\mathrm{d}^{-1}$ (Spear et al. 1981; Bossi et al. 1993). Tubbesing et al. (2000) confirmed the $1.56\,\mathrm{d}^{-1}$ frequency and found another group at about $1.60\,\mathrm{d}^{-1}$. 28 Cyg was extensively studied by Baade et al. (2018a) using photometric data from the *BRITE* and *SMEI* satellites. The variability is clustered into three frequency groups with approximate ranges 0.1–0.5, 1.0–1.7 and 2.2–$3.0\,\mathrm{d}^{-1}$. The peaks of highest amplitude occur at 1.381, 1.545 and $1.597\,\mathrm{d}^{-1}$.

Baade et al. (2018a) note that stochastic variability is an important contribution to the light curve. However, they stress that coherent variations certainly occur. They point out the clear signature of low-order g-mode pulsations in high-resolution spectra (Rivinius et al. 2003), demonstrating coherent large-scale structures in the photosphere. These observations were, necessarily, of relatively short duration so it is not entirely clear that coherence is well established.

Periodograms of the *TESS* data are shown in Fig. 2. These look very different from the *BRITE* periodograms in that the frequency spectrum is much denser. However, the three groups are still present. The three coherent peaks of largest amplitude mentioned by Baade et al. (2018a) do not seem to correspond with peaks in the *TESS* data. Either the amplitudes are lower or the frequencies are not quite as coherent as expected. Note that peaks in sector 14 look quite different from those in sector 15 and that the time-frequency diagram suggests somewhat erratic behaviour.

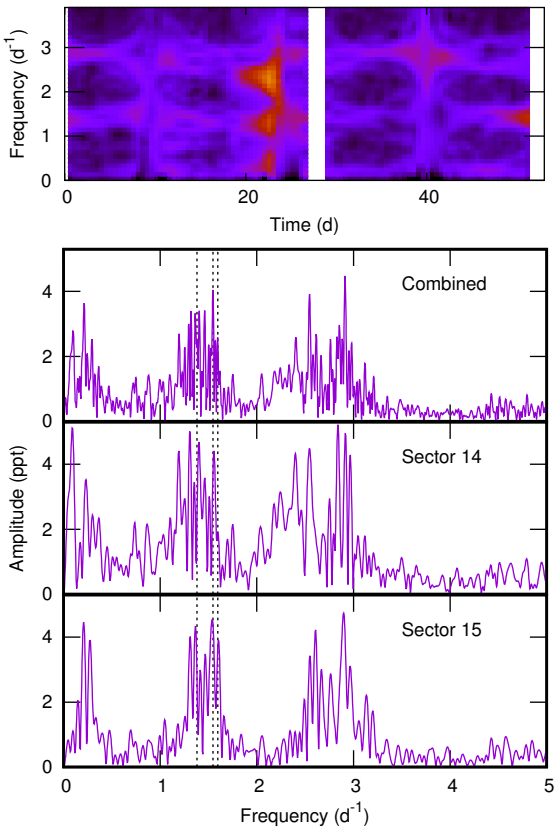

Figure 2. Time-frequency diagram and periodograms of the combined data and of individual observing sectors of TIC 42360166 (28 Cyg). The vertical dotted lines represent the frequencies 1.381, 1.545 and $1.597\,\mathrm{d}^{-1}$ mentioned by Baade et al. (2018a).

Because one frequency group is roughly twice the frequency of the other, we have assumed that the fundamental group at around $1.5\,\mathrm{d}^{-1}$ reflects the approximate rotational frequency of the star. It is well-known that Be stars vary in light over a timescale of weeks and months due to the effect of the circumstellar disc. Attributing the low-frequency group at 0.1–$0.5\,\mathrm{d}^{-1}$ to circumstellar material seems reasonable.

5.2 TIC 55295028, HD 33599

Bernhard et al. (2018) detected a frequency of $0.9051\,\mathrm{d}^{-1}$ from ground-based photometry. Balona et al. (2019) did not detect a period from *TESS* sector 1–2.

The time-frequency diagram (Fig 3) shows two groups with fundamental frequency of around $0.94\,\mathrm{d}^{-1}$ which we adopt as the rotational frequency. Three harmonics are visible as indicated by the dotted lines. There is a sudden decline in amplitude in all groups between sector 3 and 4.

There is also a low-amplitude peak at $5.171\,\mathrm{d}^{-1}$ which is first visible in sector 4 and subsequent sectors. The line

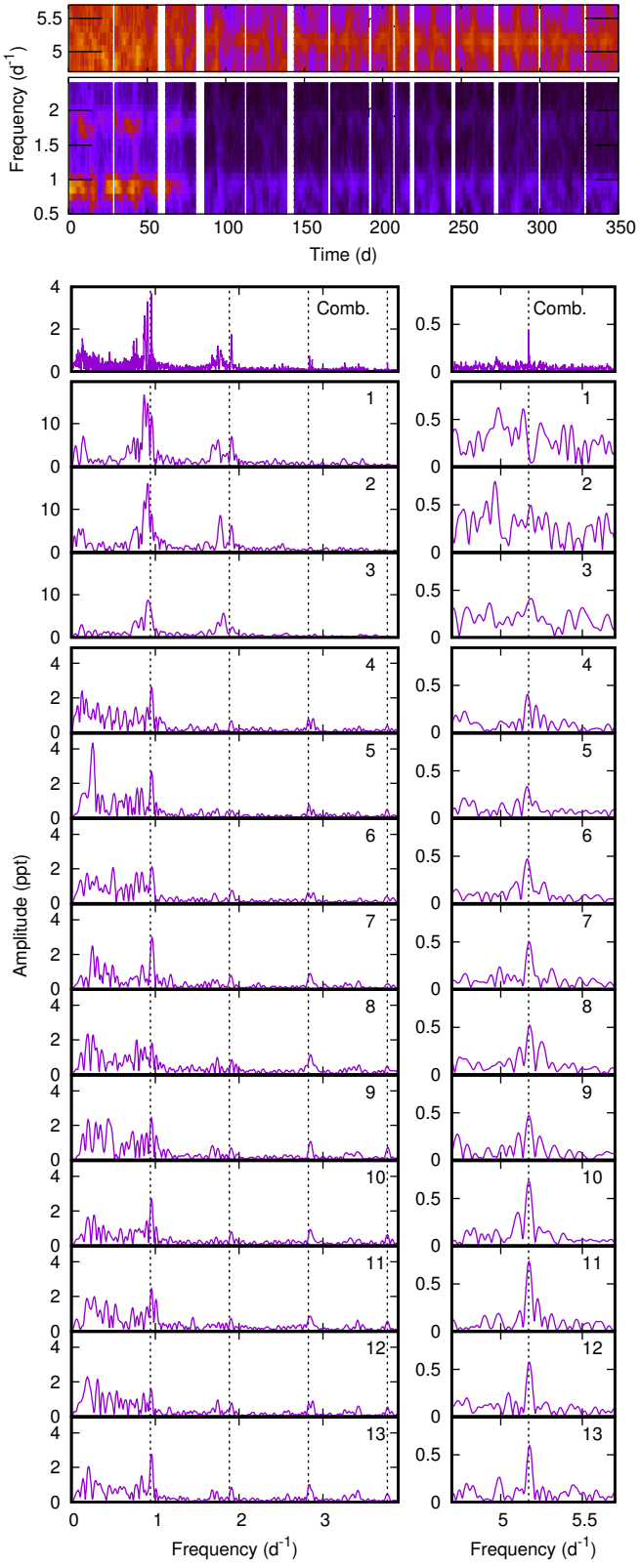

Figure 3. The time-frequency diagram and periodograms of the combined data and of individual observing sectors (labeled) of TIC 55295028. Note the changes in amplitude scale in the periodograms. The vertical dotted lines represent the frequency $\nu = 0.94\,\mathrm{d}^{-1}$ and its three harmonics on the left. The right hand panels shows the peak $\nu = 5.17141\,\mathrm{d}^{-1}$.

Table 3. Extracted frequencies, ν (d^{-1}), and amplitudes, A (ppt). The figures in brackets denote the error in the last digit.

ν	A	ν	A	ν	A
TIC 65803653 (27 CMa):					
0.7896(4)	2.09(1)	2.6793(4)	1.54(1)	13.1131(9)	0.10(1)
1.2608(4)	2.06(1)	5.1578(6)	0.35(1)	13.5096(5)	0.54(1)
1.3472(4)	1.68(1)	5.9020(7)	0.31(1)	14.7340(9)	0.11(1)
1.4060(4)	1.26(1)	10.8837(4)	1.08(1)	24.3903(9)	0.09(1)
2.6240(4)	1.88(1)				
TIC 234230792 (HD 49330):					
0.8601(7)	1.56(3)	2.9164(4)	3.34(3)	5.8908(9)	0.83(3)
2.4565(8)	1.31(3)	4.2518(7)	1.48(3)	11.8657(9)	0.77(3)
2.6044(7)	1.66(3)	4.3771(9)	0.85(3)	16.1122(9)	0.27(3)
2.7154(7)	2.39(3)				

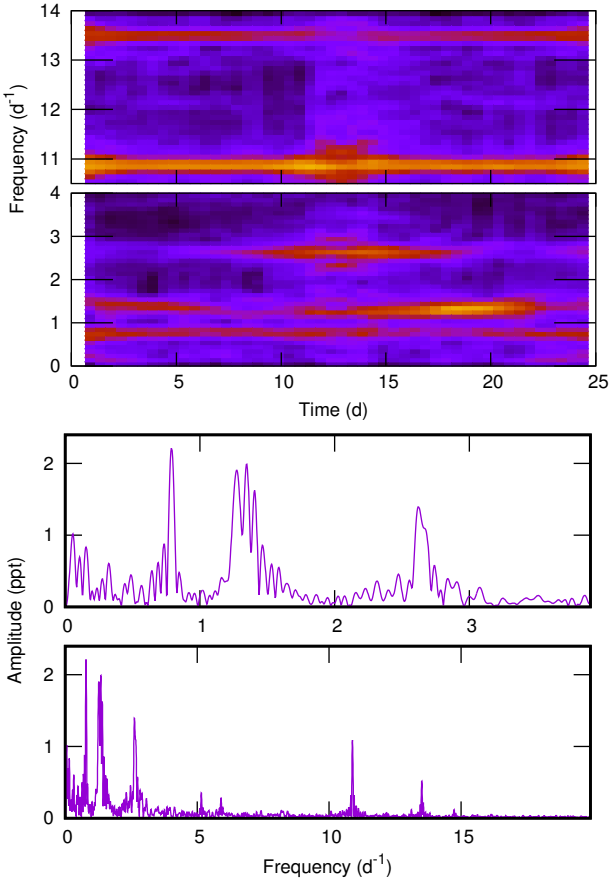

Figure 4. Time-frequency diagrams and periodograms of TIC 65803653 (27 CMa) showing high frequencies as well as variable-amplitude peaks.

is sharp and the frequency constant (right panel in Fig. 3). It does not seem to be harmonically related to the broad peak groups and is most probably due to pulsation. The star may thus be classified as a β Cep variable. It is possible that the β Cep pulsation retains constant amplitude, but the increased background noise in sectors 1–3 renders it less visible.

5.3 TIC 65803653, 27 CMa

27 CMa is a very close optical multiple system. From ground-based photometry, Balona & Rozowsky (1991) found a single frequency, $0.7925\,\mathrm{d}^{-1}$, in 1986 and 1987. When the star was next observed in 1990, in addition to the quoted frequency, a new peak at $10.8914\,\mathrm{d}^{-1}$ made its appearance. The high frequency, characteristic of a β Cep star, was still present in 1991.

The appearance of β Cep pulsations may be related to the changes in the spectrum reported by Bhattacharyya & Ghosh (1989) and Ghosh et al. (1989). Prior to the appearance of β Cep pulsations, observations showed typical double-peaked Hα emission. In early 1989 the Hα and He I λ5876 lines displayed P-Cyg profiles. Later that year, the appearance of the spectrum in the region of Hα, Si λ6347, Si λ6371 and He I λ5876 suggested that the star had entered into a shell phase.

Since self-driven pulsations are not known to appear and disappear in non-Be stars, it is perhaps possible that the pulsations were simply masked from view prior to the development of the shell phase. Once the shell phase was established, the obscuration was removed and the β Cep pulsations became visible.

The *TESS* periodogram (Fig. 4) shows multiple peaks in which β Cep pulsations are visible. A list of extracted frequencies is shown in Table 3. The peak at $10.8837\,\mathrm{d}^{-1}$ corresponds to that seen by Balona & Rozowsky (1991). The time-frequency diagram indicates variability in both amplitude and frequency in some of the low-frequency peaks. By contrast, the frequency and amplitude of the β Cep pulsations seem to be stable. The peak at $2.6\,\mathrm{d}^{-1}$ seems to be an harmonic of the broad peak at around $\nu = 1.3\,\mathrm{d}^{-1}$ which is assumed to be the rotational frequency. The nature of the $0.7896\,\mathrm{d}^{-1}$ frequency, which is the one observed by Balona & Rozowsky (1991), is not clear. It appears to be stable in both frequency and amplitude.

5.4 TIC 148917425, κ Dra

Baker (1920) found κ Dra to be a spectroscopic binary with a period of 8.986 d ($0.111\,\mathrm{d}^{-1}$). Later Hill (1926) confirmed the binary nature but with a period of 0.89038 d ($1.123\,\mathrm{d}^{-1}$) which is the 1-d alias of the period found by Baler. Juza et al. (1991) obtained further spectroscopic observations and confirmed the presence of the 0.89-d period which is transient in nature and suggested that it might be the rotation period. In addition, they found the star to be a binary with a period of 61.55 d.

The *TESS* periodograms (Fig, 5) show two broad peaks at a frequency of $\nu \approx 0.89\,\mathrm{d}^{-1}$ and its harmonic. The $0.89\,\mathrm{d}^{-1}$ peak is the 1-d alias of the $1.123\,\mathrm{d}^{-1}$ frequency found by Juza et al. (1991). The time-frequency diagram suggests that their amplitudes vary, in agreement with the transient character reported by Juza et al. (1991).

In addition, the *TESS* periodogram of the combined data shows a pair of high-frequency peaks at 34.696 and $35.744\,\mathrm{d}^{-1}$. This would suggest that κ Dra is a Maia star (Balona et al. 2016), since it is too cool for a β Cep variable.

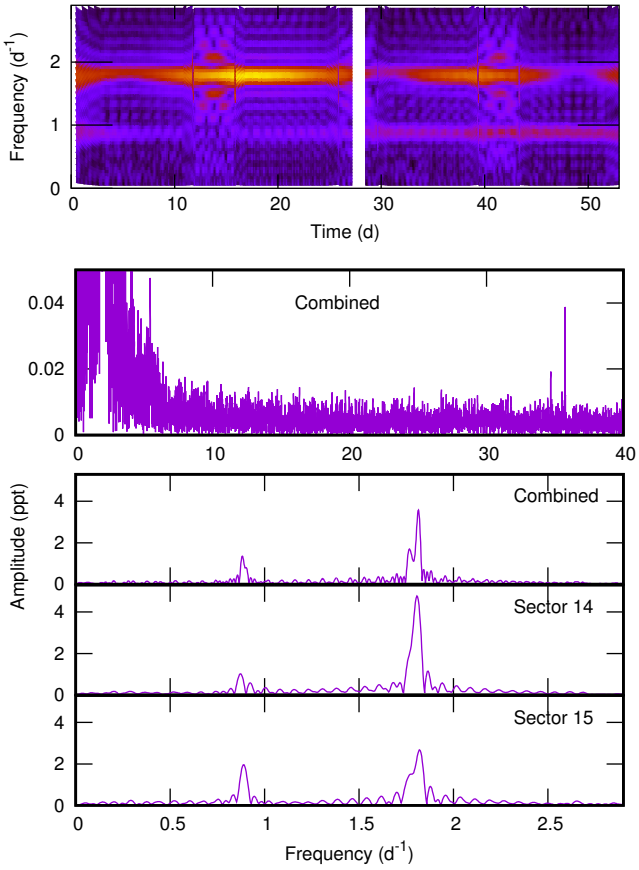

Figure 5. Time-frequency diagram and periodograms of TIC 148917425 (κ Dra) showing high frequencies (top panel) as well as variable-amplitude rotational peaks.

5.5 TIC 207176480, HIP 14595

Houk & Cowley (1975) classified HD 19818 as B9/A0Vne: with weak Balmer emission. It is an X-ray source (Nazé & Motch 2018). From ground-based *KELT* photometry, Oelkers et al. (2018) obtained a frequency of $0.7031\,\mathrm{d}^{-1}$.

Balona et al. (2019) list the star, but no periodicity was found from *TESS* sector 2 alone. The additional sector 3 observations show two strong flares at BJD 2458377.72 and BJD 2458393.80 (Fig. 6). These are probably related to the X-ray source. The flare energies are approximately 2.5×10^{37} and 1.1×10^{38} ergs or 10^7 and 10^8 more energetic than solar flares. On removing the flares, the resulting periodogram shows just a single peak at $0.2977\,\mathrm{d}^{-1}$ (amplitude 2.740 ppt). The *KELT* frequency is the 1-d alias of the this frequency. This is assumed to be the rotational frequency, but it could also be an orbital frequency in which the secondary is involved in generating the X-rays and flares. The projected rotational velocity is not known. It would be important to obtain more detailed spectroscopic observations of this interesting star.

5.6 TIC 230981971, α Eri

Achernar (HD 10144) is the brightest and the nearest Be star in the sky. Using Earth-rotation synthesis on the *VLT*

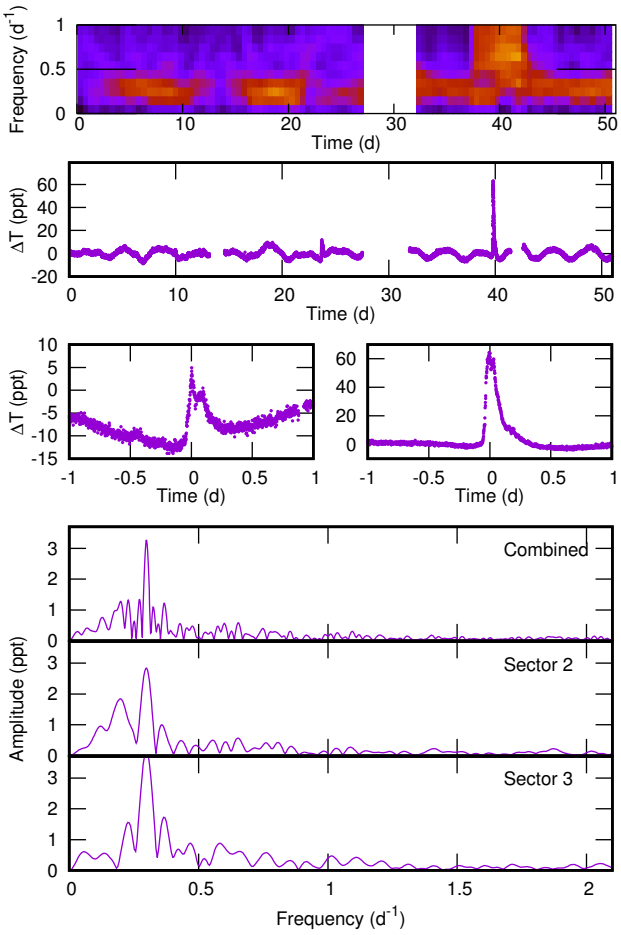

Figure 6. The top panel is time-frequency diagram of TIC 207176480 (HD 19818) showing amplitude changes in the 0.2977 d^{-1} frequency. The next three panels show the light curve and detail of two flares. The bottom three panels show periodograms of the combined data and periodograms of data in two sectors.

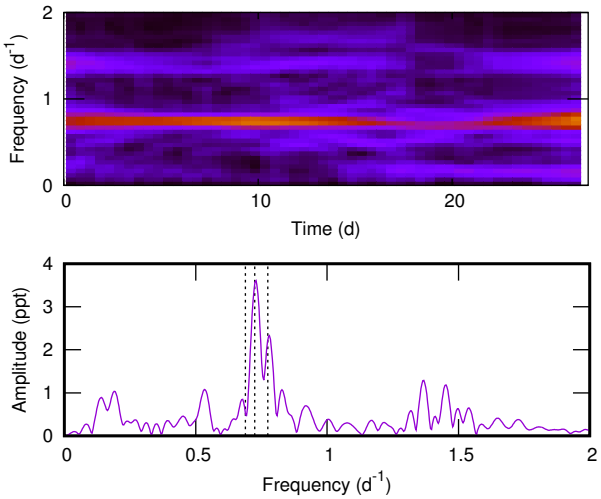

Figure 7. The top panel shows the time-frequency diagram of TIC 230981971 (α Eri) from *TESS* sector 2 data. The bottom panel is the corresponding periodogram. The dotted lines are the frequencies 0.689, 0.725 and 0.775 d^{-1} found by Goss et al. (2011).

interferometer, Domiciano de Souza et al. (2003) measured an oblateness of 1.56 ± 0.05. The star has a companion, most likely an A1V–A3V star, with an orbital period of about 15 yr (Kervella et al. 2008).

The first indication of short-period variations was a photometric/spectroscopic study by Balona et al. (1987) who found a frequency of 0.79 d^{-1}. From line profile observations,Rivinius et al. (2003) obtained 0.77 d^{-1}. Goss et al. (2011) analysed photometry from the *SMEI* instrument in yearly 50-d segments over a 5-yr period. They found frequencies of 0.725, 0.775 and one of much lower amplitude at 0.689 d^{-1}, all with variable amplitudes. The 0.775 d^{-1} frequency appears to be coherent over the whole period, while the 0.725 d^{-1} frequency did not exhibit coherence. Balona et al. (2019) did not detect a period from *TESS* sector 2.

The periodogram from one sector of *TESS* observations show two peak groupings at around 0.73 and 1.46 d^{-1}. Each group shows multiple closely-spaced peaks (Fig. 7). The *TESS* periodogram is very similar to the one obtained by Goss et al. (2011) and the frequencies at 0.725 and 0.775 d^{-1} seem to be still present (dotted lines in the figure). Judging from the time-frequency diagram, amplitude variations are present in both frequency groups. The peaks at 1.45 d^{-1} also appear to change frequency.

Domiciano de Souza et al. (2014) derive the stellar parameters from interferometric observations, finding an equatorial radius $R_{\rm eq} = 9.16 \pm 0.20 R_\odot$. They adopt 0.689 d^{-1} as the rotational frequency, which is the lowest-amplitude frequency found by Goss et al. (2011), because it fits better with their calculations. This leads to $v/v_c \approx 0.81$. If we assume that 0.73 d^{-1} represents the rotational frequency (with the 1.46 d^{-1} the first harmonic) and a radius of 9.16 $R_\odot$, an equatorial rotational velocity of 340 km s^{-1} and $v/v_c \approx 0.74$ is obtained. The projected rotational velocity is $v \sin i = 260 \pm 15$ km s^{-1} (Domiciano de Souza et al. 2014).

The actual $v \sin i$ of Achernar seems to significantly vary in time, as shown by Rivinius et al. (2013). The reported values span the range 223–290 km s^{-1}. The value appears to correlate with the disk emission, being higher at when emission is strongest. It is interpreted as a variation of the equatorial rotation rate of photospheric layers and further elaborated by Rivinius et al. (2016a).

5.7 TIC 234230792, HD 49330

HD 49330 was observed by the *CoRoT* mission for nearly 137 d during 2007–2008, as described by Huat et al. (2009). During this time the star underwent a mini outburst where the brightness increased by 0.03 mag over the course of a 20-d period (Fig. 8). Prior to, during, and after the outburst, Huat et al. (2009) identify four phases as shown in Fig. 8.

The periodogram of the *TESS* data, also shown in Fig 8, closely resembles the outburst phase. Extracted frequencies are listed in Table 3. Note that the high-frequency β Cep pulsations visible in the *CoRoT* data have very low amplitudes in the *TESS* data. This may be due to an active obscuration phase during the *TESS* observations (described below) or it

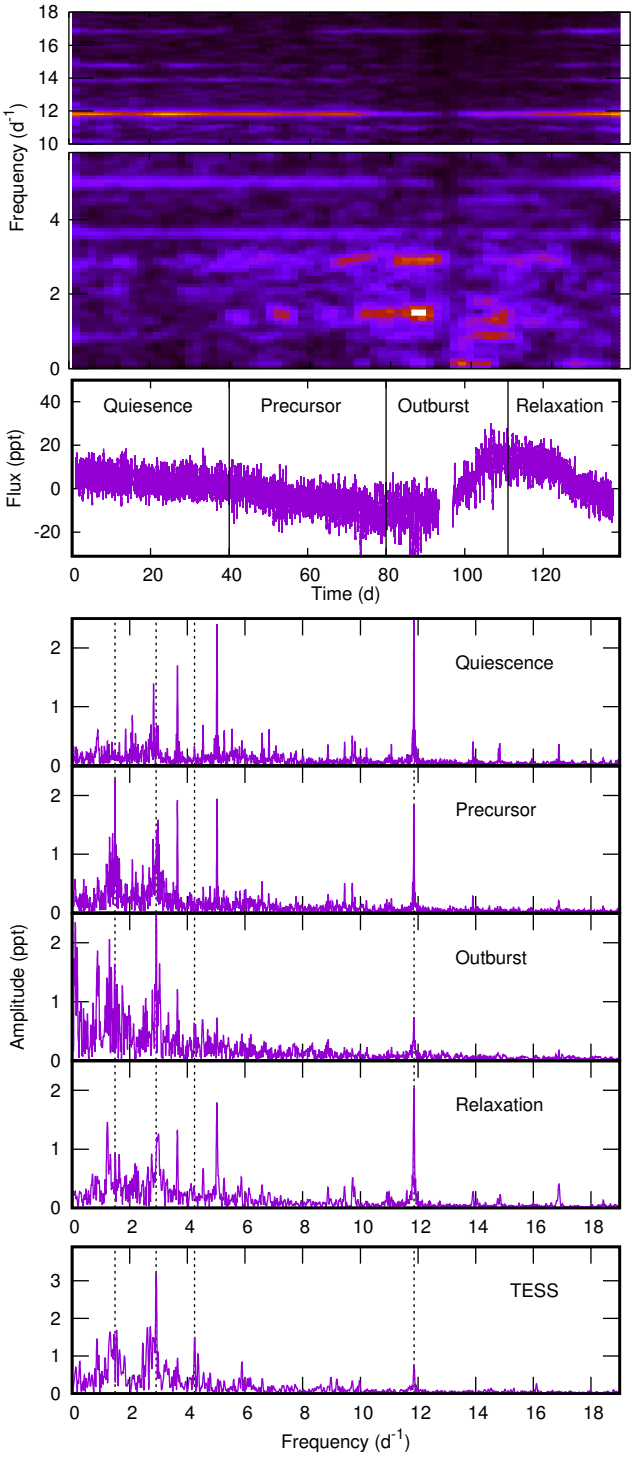

Figure 8. The top panels are time-frequency diagrams for *CoRoT* observations of TIC 234230792 (HD 49330). The next panel is the *CoRot* light curve showing four phases of the mini-outburst. Below this panel, the *CoRoT* periodograms corresponding to each outburst phase are shown. The bottom panel is the *TESS* sector 6 periodogram. The dotted lines are at frequencies 1.4934, 2.9164, 4.2518 and 11.8657 d^{-1}.

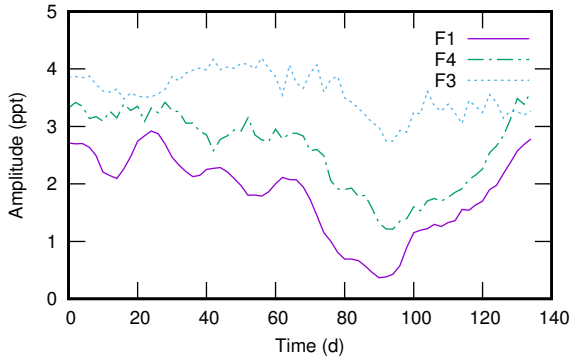

Figure 9. Variation of the amplitudes of the β Cep modes with frequencies $F1 = 11.8639$, $F3 = 3.6594$ and $F4 = 5.0260\,\mathrm{d}^{-1}$ as a function of time from the *CoRoT* data of HD 49330. The amplitudes have been arbitrarily displaced to reduce confusion.

may be a result of the different passbands in *CoRoT* and *TESS*.

During the precursor and outburst phases two groups of peaks around 1.47 and 2.94 d^{-1} gradually emerge. In addition, a more concentrated group around 0.87 and 1.28 d^{-1} also makes its appearance. The amplitudes of the high-frequency β Cep pulsations at 11.86 and 5.03 d^{-1} decrease remarkably during the outburst phase.

Huat et al. (2009) interpret the peak groups around 1.47 and 2.94 d^{-1} as systems of closely-spaced g modes. They find a correlation between both amplitude changes and the presence/absence of certain frequencies of pulsations at the different phases of the outburst. The amplitudes of the main frequencies (the β Cep pulsations) decrease before and during the outburst and increase again after the outburst. Also, several groups of frequencies (g modes) appear just before the outburst, reach maximum amplitude during the outburst and then disappear as soon as the outburst has finished. As already mentioned, these are interpreted as g modes with short lifetimes. They suggest that the frequency group around 0.87 d^{-1}, which is compatible with the rotational frequency, could be explained by the ejection of material co-rotating with the star.

The interpretation by Huat et al. (2009) is in line with the common view that NRP is the cause of the mass loss (Rivinius et al. 1998). The idea is that the sudden large increase in pulsation amplitudes of the groups around 1.47 and 2.94 d^{-1} is responsible for the ejection of material. The decrease in amplitude shortly afterwards shuts off further mass loss.

In our view, this interpretation is not consistent with the available information. In the first place, it is clear that Be stars, in general, do not rotate very close to the critical rotation rate, as required by the notion that pulsation acts as a trigger for mass loss. Also, the so-called g-mode groups around 1.47 and 2.94 d^{-1} appear to be non-coherent as is evident from the time-frequency diagram of Fig. 8. Note the appearance of these frequency groups compared to the smooth appearance of the β Cep pulsations at 3.6594, 5.0260 and 11.8639 d^{-1}.

Huat et al. (2009) explain the decrease and subsequent increase of the β Cep pulsations as an actual variation of pulsation amplitude, though no reason is given for such an

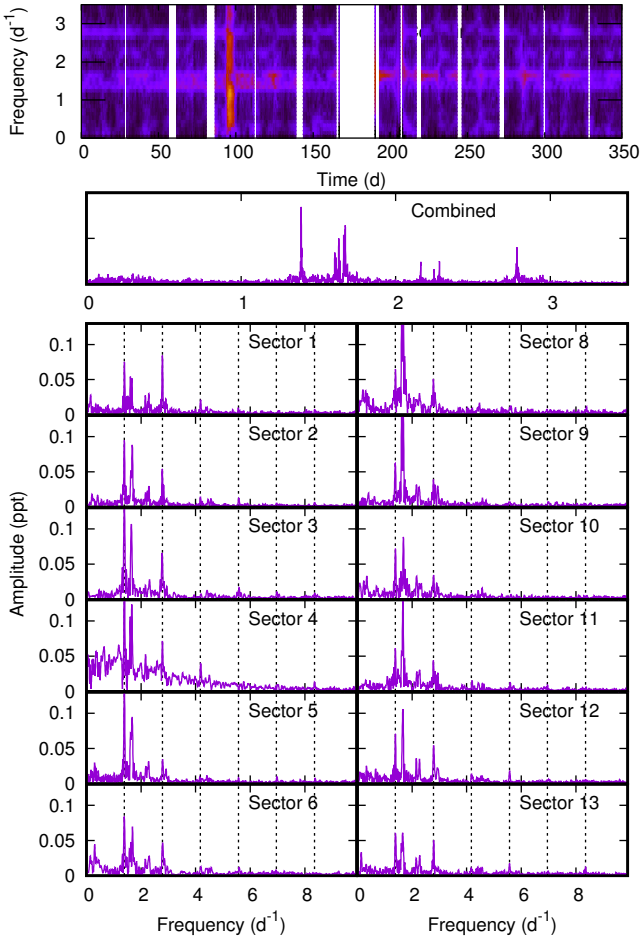

Figure 10. Time-frequency diagram and periodograms of the combined data and of individual observing sectors of TIC 260640910 (μ Pic). The dotted lines show $\nu = 1.38854(1)\,\mathrm{d}^{-1}$ and 5 harmonics.

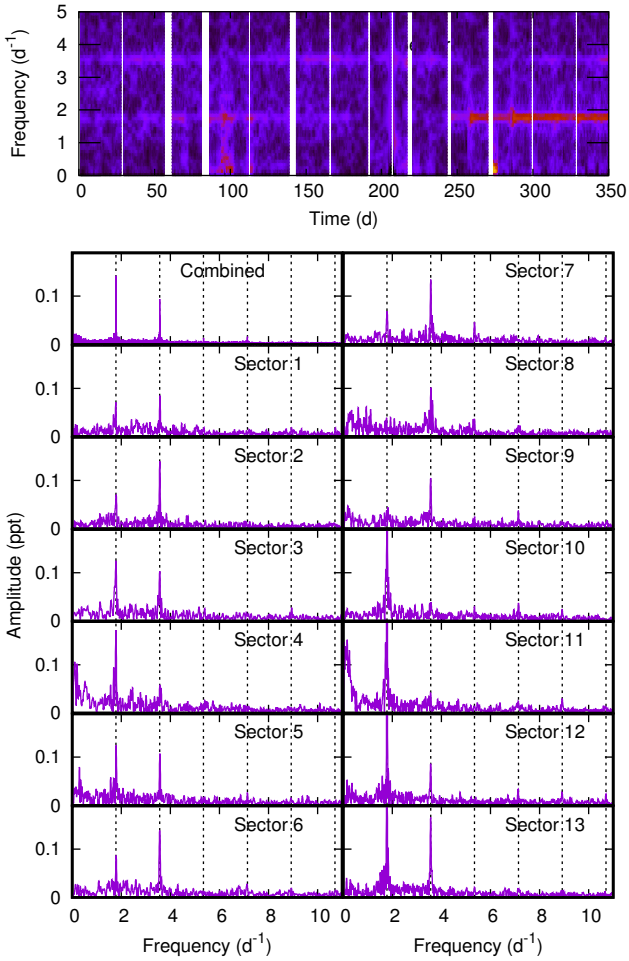

Figure 11. Time-frequency diagram and periodograms of the combined data and of individual observing sectors of TIC 279430029. The vertical dotted lines represent the frequency $\nu = 1.784\,\mathrm{d}^{-1}$ and its harmonics.

amplitude change. Amplitude variation in all known self-excited pulsating stars occur over timescales of many months to years and never in just a few days. We suggest that the temporary amplitude decrease is just an obscuration effect. This is demonstrated by the fact that all three β Cep modes vary in the same ratio, as shown in Fig. 9. The low amplitude of F3 and contamination from the high background makes it difficult to trace its amplitude variation, but the trend is clearly present. If this is a real variation in pulsation amplitudes, then all three independent pulsation modes have the same damping and growth rates, which is exceedingly unlikely.

5.8 TIC 260640910, μ Pic

The shell star μ Pic is a double star (B9IVn + A8V:p) with a separation of 2.4 arcsec and a magnitude difference of 3.2 mag. Balona et al. (1992) found a frequency of $2.52\,\mathrm{d}^{-1}$ from ground-based photometry. The first two *TESS* sectors were analysed by Balona et al. (2019), but no periodicity was found.

The periodogram of all 12 sectors (Fig. 10) shows multiple peaks characteristic of an SPB pulsating variable. The main peak at $1.392\,\mathrm{d}^{-1}$ (amplitude 0.08 ppt) appears to be slightly broadened or double and of variable amplitude. This does not bear any relationship to the frequency mentioned by (Balona et al. 1992). Up to 5 harmonics are visible as shown in Fig. 10, each harmonic being rather broad. This may be the rotational frequency. A secondary peak system at about $1.63\,\mathrm{d}^{-1}$ consists of multiple peaks of variable amplitude which may be due to g-mode pulsations. For this reason we classify the star as SPB+ROT.

5.9 TIC 279430029, HD 53048

Balona et al. (2019) found a frequency of $1.784\,\mathrm{d}^{-1}$ and its harmonic from first-light *TESS* observations. The periodogram of the complete data set (13 sectors) confirms a broad or unresolved main peak at this frequency with amplitude of 0.14 ppt. Five harmonics are visible and we assume $1.784\,\mathrm{d}^{-1}$ to be the rotational frequency. The amplitude of the fundamental peak and its harmonics change quite dramatically from sector to sector, as shown in Fig. 11.

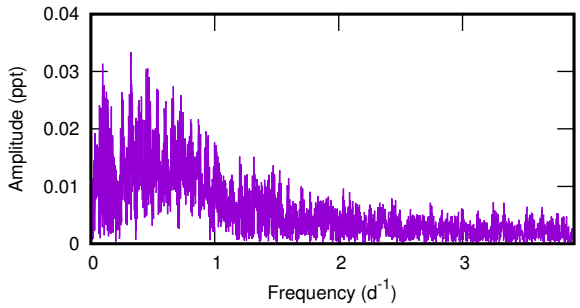

Figure 12. Periodogram of combined data for TIC 308748912.

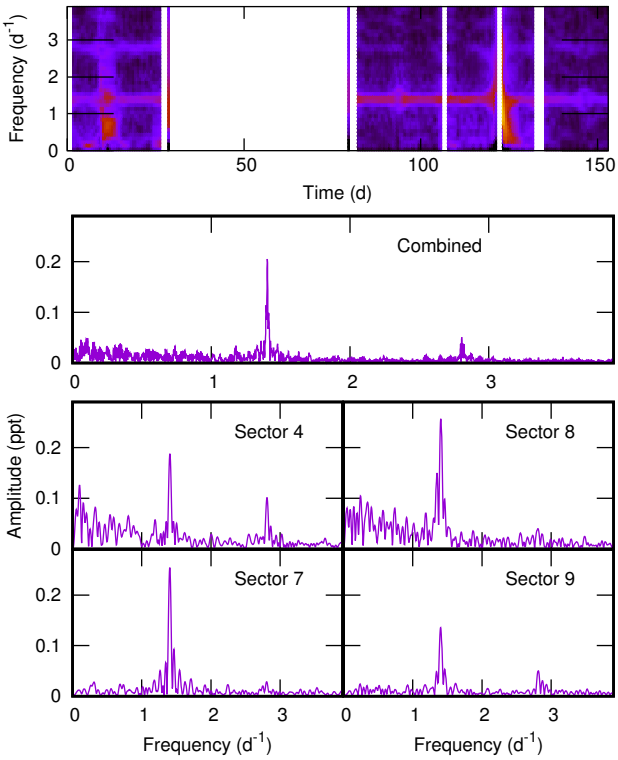

Figure 13. Time-frequency diagram and periodograms of the combined data and of individual observing sectors of TIC 341040849.

On occasions (sectors 8 and 9), the fundamental disappears altogether, resulting in a double-wave light curve.

5.10 TIC 308748912, HR 3217

This is a poorly studied B6V or B7IVek star with narrow lines ($v \sin i = 26\,\mathrm{km}^{-1}$; Zorec & Royer 2012). A study of the first two sectors from *TESS* by Balona et al. (2019) showed no significant periodicity The addition of four further sectors does not change this assessment (Fig. 12). While this star appears to be uninteresting, it presents an important challenge in understanding how mass loss can arise in a star which seems to lack any activity.

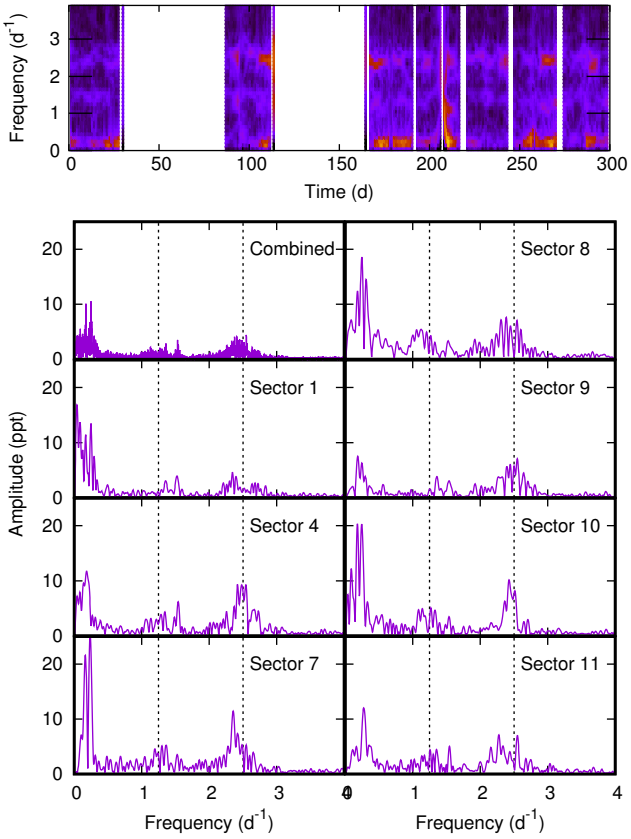

Figure 14. Time-frequency diagram and periodograms of the combined data and of individual observing sectors of TIC 364398342. The vertical dotted lines represent the frequency $\nu = 1.25\,\mathrm{d}^{-1}$ and its harmonic.

5.11 TIC 341040849, HIP 38433

This poorly-studied star is a member of NGC 2516. A peak at $1.406\,\mathrm{d}^{-1}$ and its harmonic are visible (Fig. 13). Both peaks are rather broad and variable in amplitude. This simple frequency spectrum is similar to that in TIC 55295028 (Fig. 3), κ Dra (Fig. 5) and TIC 279430029 (Fig. 11). The light curve is almost sinusoidal as in η Cen (Baade et al. 2016) and ν Pup (Baade et al. 2018b). Light curves showing a broad or very closely spaced multiple peaks and its harmonic are common and describe about 40 percent of the Be stars in our sample, as discussed later. They seem to be mostly mid- or late-B stars.

5.12 TIC 364398342, V374 Car

This star is a member of the open cluster NGC 2516 (Sampedro et al. 2017) and also an X-ray source (Nazé & Motch 2018). From its position in the H-R diagram it can be classified as a blue straggler (Ahumada & Lapasset 2007) and may be a spectroscopic binary (González & Lapasset 2000). The star was discussed by Balona et al. (2019) but no periodicity was mentioned.

The time-frequency diagram and periodograms in Fig. 14 shows two broad peaks at about 1.25 and $2.50\,\mathrm{d}^{-1}$ as well as structure at very low frequencies. No resolved

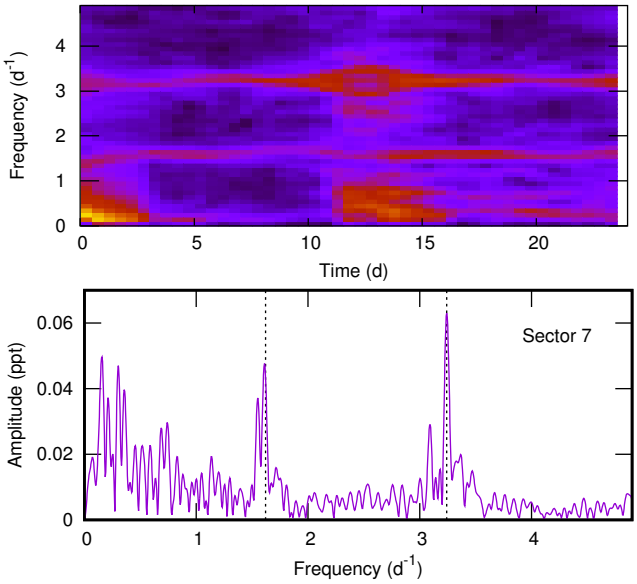

Figure 15. Time-frequency diagram and periodograms of β CMi. The dotted lines represent the assumed rotational frequency $1.621\,\mathrm{d}^{-1}$ and its first harmonic.

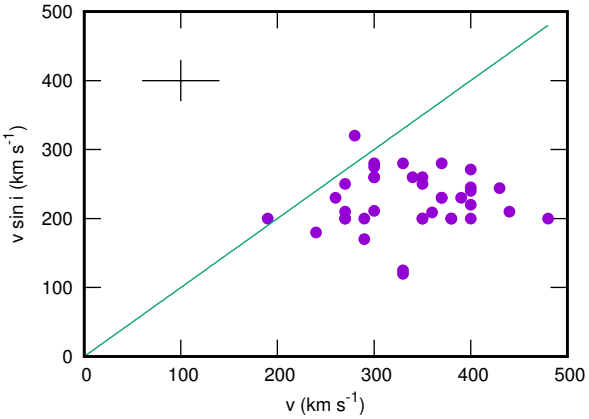

Figure 16. The projected rotational velocity, $v \sin i$, as a function of the equatorial rotational velocity, v, for the Be stars observed by *TESS*. The straight line represents $\sin i = 1$. Typical error bars for each point are shown by the cross.

feature can be seen. Broad peaks such as these are found in several Be stars such as KIC 6954726 and KIC 11971405 (Rivinius et al. 2016b). It is possible that the broadening is simply a result of incoherence associated with co-rotating gas clouds close to the photosphere and that the $1.25\,\mathrm{d}^{-1}$ measures the approximate rotation frequency of the star.

5.13 TIC 425224332, β CMi

Saio et al. (2007) analysed photometry of β CMi from the *MOST* satellite and concluded that it is a multiperiodic non-radial pulsator. In a re-analysis of the same data, Harmanec et al. (2019) did not find any coherent frequency. The dominant frequency of $3.257\,\mathrm{d}^{-1}$ appears to vary in frequency around its mean value. They conclude that there is only one stable frequency of $1.621\,\mathrm{d}^{-1}$ which they associate with the rotational frequency.

The *TESS* time-frequency diagram and periodogram is show in Fig. 15. The peak at around $1.61\,\mathrm{d}^{-1}$ is double, but this is due to slight frequency variations as can be seen by close inspection of the time-frequency diagram. The peak around $3.35\,\mathrm{d}^{-1}$ is equally variable in frequency and amplitude. There are indications of the 4th and 6th harmonics as well. Most likely, this is another case of a star in which the rotational frequency, $1.621\,\mathrm{d}^{-1}$, and its harmonic is present.

During the *MOST* observations, this frequency had very low amplitude and the light curve was dominated by the first harmonic, giving a double-wave variation. At that time, the first harmonic could have mistakenly taken as the rotational frequency. In the *TESS* data, the light curve has unequal minima so that the true rotation frequency is revealed.

6 DISCUSSION

In the Appendix, periodograms of the remaining *TESS* Be stars are presented. Out of the 57 stars in our sample, 25 have a simple periodogram consisting of a peak and its harmonic, or in some stars, several harmonics. The peak may be somewhat broadened or with fine structure. In a further 18 stars, the peaks cluster in groups which have an harmonic relationship. The peak frequencies are different from sector to sector. Often the peaks are broad. All this points to non-coherent variations arising from circumstellar material.

On the assumption that the fundamental frequency of the group is the rotational frequency, approximate rotational frequencies for 42 stars (i.e. 74 percent of the sample) can be determined. These are listed in Table 1. Of the remaining 14 stars, 6 are β Cep, SPB, Maia or δ Sct pulsating variables. The other stars just show low frequency variations which may possibly be attributed to circumstellar material.

In the 42 stars where periodicity can be found, the fundamental is usually the dominant peak, but the first harmonic has higher amplitude in about one-third of the stars. This ratio may vary quite considerably from time to time, as mentioned above. The tendency for Be stars to show such frequency groups, can be understood in the context of the working model described in Section 2.

A large fraction of non-Be stars also show rotational modulation and it is reasonable to suppose that Be stars are no different. However, the typical amplitude in Be stars (around 1 ppt) is about an order of magnitude larger than in normal B stars (about 0.1 ppt; Balona 2019). This is in line with our working model in which most of the periodic variation is attributed to trapped matter and not starspots.

If rotation is indeed responsible for the quasi-periodic light variations, then the equatorial rotational velocity, v, estimated from the photometric period and the radius, should be related to the projected rotational velocity, $v \sin i$. A plot of $v \sin i$ as a function of v (Fig. 16) shows that this is indeed the case. Within the measured error, $v \sin i < v$ for all stars.

It should be noted that the error in v is considerable, as shown by the error bars in Fig. 16. Systematic errors in v are also likely to be present because the radius was derived from

the effective temperature and luminosity. The derived effective temperatures for Be stars are not only poorly known, but probably somewhat cooler than the actual effective temperature because it is mostly the gravity-darkened equatorial region that is observed. Thus the radius is probably overestimated, leading to larger v for the more rapidly-rotating stars.

Many stars are probably unresolved multiple systems. While the *GAIA* parallax will be unaffected, the apparent brightness, and hence the derived luminosity and radius, will be larger than that of a single star. Thus the estimated v will tend to be larger than its true value. On the other hand, polar flattening due to rapid rotation means that the estimated equatorial radius, and hence v, is likely to be too low for the most rapidly rotating stars. The last factor probably compensates to some extent the tendency towards a v estimate which is too large. At present, *GAIA* parallaxes offer the best estimate of the equatorial rotational velocity, but the effect of possible multiplicity remains a concern.

7 CONCLUSIONS

While non-radial pulsation has long been viewed as a possible cause for mass loss in Be stars, recent analysis of the equatorial velocity distribution by Cranmer (2005) and Zorec et al. (2016) suggests that most Be stars rotate well below the critical velocity. Since the NRP model requires near-critical rotation, these results pose a problem.

Recent photometry from space has shown that a large fraction of A and B stars show what appears to be rotational modulation (Balona 2019). This suggests that the long-held assumption of quiescent envelopes in stars with radiative envelopes, free of magnetic fields, requires revision. In this light, we present a working model, first proposed by Balona (2003), designed to overcome the limitations presented by NRP.

In the search for further clues and to test the new model, we have examined in some detail the light curves of 57 classical Be stars observed by the *TESS* satellite.

It is found that the most common light curve (about 40 percent) among Be stars is a simple single- or double-wave sinusoid. In the periodogram this appears as a slightly broadened peak, or peak with fine structure, and its first harmonic. The relative strengths of the first and second harmonics vary on a timescale of months to years. Stars showing this light curve morphology tend to be mid- to late-B stars.

In about 30 percent of Be stars, the periodogram still shows a fundamental and first harmonic, but with multiple peaks which form frequency groups. It seems that none of these multiple peaks are coherent since the appearance of the periodogram varies on timescales of months. These tend to be mostly mid- to early B stars.

In about 74 percent of Be stars, a fundamental and first harmonic can be identified in the periodogram. Comparison of the derived equatorial rotational velocity, v, with the projected rotational velocity, $v \sin i$, shows that assumption of rotational modulation in these stars is consistent with observations.

Observations of HD 49330 by *CoRoT* and discussed by Huat et al. (2009) offer a particularly interesting insight to the mass loss mechanism and the physical processes during an outburst. This star is also a β Cep pulsating variable. It turns out that just after the outburst there is a significant reduction and subsequent recovery of the amplitudes of these pulsations.

The most important result is that the amplitudes of the two modes of highest amplitude, and possibly a third mode, decrease and increase with time in the same ratio. This could be explained if the damping and driving coefficients are the same for each mode, which does not seem likely. Moreover, the timescale of the amplitude variation is shorter than in any other pulsating variable.

Our proposal is that the pulsation amplitudes remain the same throughout the whole time sequence. We suggest that shortly after the outburst, some of the ejected material changes its state and becomes optically thick, masking the underlying photosphere. As it dissipates, the pulsations regain their previous amplitudes. The temporary obscuration thus produced would account in a simple way for the variation of amplitude and the short timescale. Ground-based observations of 27 CMa may show the same effect, but unfortunately the poor coverage does not allow any definite deductions to be made.

Be stars are clearly very complex and exhibit a huge range of physical processes. The study of the light curves, while important in providing constraints, cannot by itself provide sufficient information to reveal these processes. We still do not understand the connection between the quasi-periodic variations which occur close to the photosphere and the circumstellar disc. Further progress will require not only long-term photometric monitoring from space, but simultaneous spectroscopic observations as well.

ACKNOWLEDGMENTS

LAB wishes to thank the National Research Foundation of South Africa for financial support. Funding for the *TESS* mission is provided by the NASA Explorer Program. Funding for the *TESS* Asteroseismic Science Operations Centre is provided by the Danish National Research Foundation (Grant agreement no.: DNRF106), ESA PRODEX (PEA 4000119301) and Stellar Astrophysics Centre (SAC) at Aarhus University.

This work has made use of data from the European Space Agency (ESA) mission Gaia, processed by the Gaia Data Processing and Analysis Consortium (DPAC). Funding for the DPAC has been provided by national institutions, in particular the institutions participating in the Gaia Multilateral Agreement.

This research has made use of the SIMBAD database, operated at CDS, Strasbourg, France. Data were obtained from the Mikulski Archive for Space Telescopes (MAST). STScI is operated by the Association of Universities for Research in Astronomy, Inc., under NASA contract NAS5-2655.

REFERENCES

Ahumada J. A., Lapasset E., 2007, A&A, 463, 789
Arcos C., Kanaan S., Chávez J., Vanzi L., Araya I., Curé M., 2018, MNRAS, 474, 5287
Baade D., et al., 2016, A&A, 588, A56

Baade D., et al., 2018a, A&A, 610, A70
Baade D., et al., 2018b, A&A, 620, A145
Baker R. H., 1920, Publications of the Astronomical Observatory of Michigan, 3, 29
Balona L. A., 1994, MNRAS, 268, 119
Balona L. A., 2003, in L. A. Balona, H. F. Henrichs, & R. Medupe ed., Astronomical Society of the Pacific Conference Series Vol. 305, Astronomical Society of the Pacific Conference Series. pp 263–+
Balona L. A., 2013, MNRAS, 431, 2240
Balona L. A., 2016, MNRAS, 457, 3724
Balona L. A., 2017, MNRAS, 467, 1830
Balona L. A., 2019, MNRAS, 490, 2112
Balona L. A., Rozowsky J., 1991, MNRAS, 251, 66P
Balona L. A., Engelbrecht C. A., Marang F., 1987, MNRAS, 227, 123
Balona L. A., Sterken C., Manfroid J., 1991, MNRAS, 252, 93
Balona L. A., Cuypers J., Marang F., 1992, A&AS, 92, 533
Balona L. A., et al., 2016, MNRAS, 460, 1318
Balona L. A., et al., 2019, MNRAS, 485, 3457
Barrera L. H., Mennickent R. E., Vogt N., 1991, Ap&SS, 185, 79
Bernhard K., Otero S., Hümmerich S., Kaltcheva N., Paunzen E., Bohlsen T., 2018, MNRAS, 479, 2909
Bhattacharyya J. C., Ghosh K. K., 1989, IAU Circ., 4777, 3
Boashash B., ed. 2015, Time-Frequency Signal Analysis and Processing: A Comprehensive Reference UK : Academic Press
Bossi M., Guerrero G., Zanin F., 1993, A&A, 269, 343
Cameron C., et al., 2008, ApJ, 685, 489
Cantiello M., Braithwaite J., 2011, A&A, 534, A140
Cantiello M., Braithwaite J., 2019, ApJ, 883, 106
Cantiello M., et al., 2009, A&A, 499, 279
Carrier F., Burki G., Richard C., 1999, A&A, 341, 469
Carrier F., Burki G., Burnet M., 2002, A&A, 385, 488
Chini R., Hoffmeister V. H., Nasseri A., Stahl O., Zinnecker H., 2012, MNRAS, 424, 1925
Cochetti Y. R., Arcos C., Kanaan S., Meilland A., Cidale L. S., Curé M., 2019, A&A, 621, A123
Cranmer S. R., 2005, ApJ, 634, 585
Cuypers J., Balona L. A., Marang F., 1989, A&AS, 81, 151
Domiciano de Souza A., Kervella P., Jankov S., Abe L., Vakili F., di Folco E., Paresce F., 2003, A&A, 407, L47
Domiciano de Souza A., et al., 2014, A&A, 569, A10
Eiroa C., et al., 2016, A&A, 594, L1
Gaia Collaboration et al., 2016, A&A, 595, A1
Gaia Collaboration et al., 2018, A&A, 616, A1
Ghosh K. K., Kuppuswamy K., Bhattacharyya J. C., 1989, IAU Circ., 4881, 3
Głębocki R., Gnaciński P., 2005, in Favata F., Hussain G. A. J., Battrick B., eds, ESA Special Publication Vol. 560, 13th Cambridge Workshop on Cool Stars, Stellar Systems and the Sun. p. 571
Gontcharov G. A., 2017, Astronomy Letters, 43, 472
González J. F., Lapasset E., 2000, AJ, 119, 2296
Goss K. J. F., Karoff C., Chaplin W. J., Elsworth Y., Stevens I. R., 2011, MNRAS, 411, 162
Grunhut J. H., et al., 2017, MNRAS, 465, 2432
Hahula M. E., Gies D. R., 1994, in Balona L. A., Henrichs H. F., Le Contel J. M., eds, IAU Symposium Vol. 162, Pulsation; Rotation; and Mass Loss in Early-Type Stars. p. 100
Harmanec P., et al., 2019, ApJ, 875, 13
Hill S. N., 1926, Publications of the Dominion Astrophysical Observatory Victoria, 3, 349
Houk N., Cowley A. P., 1975, University of Michigan Catalogue of two-dimensional spectral types for the HD stars. Volume I.
Huat A., et al., 2009, A&A, 506, 95
Hubrig S., Ilyin I., Kholtygin A. F., Schöller M., Skarka M., 2017, Astronomische Nachrichten, 338, 926
Jenkins J. M., et al., 2016, in Software and Cyberinfrastructure for Astronomy IV. p. 99133E, doi:10.1117/12.2233418
Juza K., Harmanec P., Hill G. M., Tarasov A. E., Matthews J. M., Tuominen I., Yang S., 1991, Bulletin of the Astronomical Institutes of Czechoslovakia, 42, 39
Kervella P., Domiciano de Souza A., Bendjoya P., 2008, A&A, 484, L13
Kholtygin A. F., et al., 2017, in Balega Y. Y., Kudryavtsev D. O., Romanyuk I. I., Yakunin I. A., eds, Astronomical Society of the Pacific Conference Series Vol. 510, Stars: From Collapse to Collapse. p. 261
Kilkenny D., Muller S., 1989, South African Astronomical Observatory Circular, 13, 69
Levenhagen R. S., Leister N. V., 2006, MNRAS, 371, 252
Lomb N. R., 1976, Ap&SS, 39, 447
Maíz Apellániz J., et al., 2019, A&A, 626, A20
Mason B. D., Hartkopf W. I., Tokovinin A., 2010, AJ, 140, 735
Nazé Y., Motch C., 2018, A&A, 619, A148
Neiner C., et al., 2009, A&A, 506, 143
Neiner C., de Batz B., Cochard F., Floquet M., Mekkas A., Desnoux V., 2011, AJ, 142, 149
Oelkers R. J., et al., 2018, AJ, 155, 39
Owocki S. P., 2004, in Maeder A., Eenens P., eds, IAU Symposium Vol. 215, Stellar Rotation. p. 515
Ozuyar D., Caliskan S., Stevens I. R., Elmasli A., 2018, Publ. Astron. Soc. Australia, 35
Pavlovski K., Ruzic Z., 1990, A&A, 236, 393
Pecaut M. J., Mamajek E. E., 2013, ApJS, 208, 9
Peters G. J., Penrod G. D., 1988, in ESA Special Publication. pp 117–120
Peters G. J., Wang L., Gies D. R., Grundstrom E. D., 2016, ApJ, 828, 47
Porter J. M., Rivinius T., 2003, PASP, 115, 1153
Ramiaramanantsoa T., et al., 2014, MNRAS, 441, 910
Ramiaramanantsoa T., et al., 2018, MNRAS, 473, 5532
Rivinius T., 2013, in Suárez J. C., Garrido R., Balona L. A., Christensen-Dalsgaard J., eds, Astronomical Society of the Pacific Conference Series Vol. 31, Stellar Pulsations: Impact of New Instrumentation and New Insights. p. 253 (arXiv:1210.0784), doi:10.1007/978-3-642-29630-7_46
Rivinius T., Baade D., Stefl S., Stahl O., Wolf B., Kaufer A., 1998, A&A, 333, 125
Rivinius T., Baade D., Štefl S., 2003, A&A, 411, 229
Rivinius T., Baade D., Townsend R. H. D., Carciofi A. C., Štefl S., 2013, A&A, 559, L4
Rivinius T., Townsend R. H. D., Baade D., Carciofi A. C., Leister N., Štefl S., 2016a, in Sigut T. A. A., Jones C. E., eds, Astronomical Society of the Pacific Conference Series Vol. 506, Bright Emissaries: Be Stars as Messengers of Star-Disk Physics. p. 17 (arXiv:1602.03452)
Rivinius T., Baade D., Carciofi A. C., 2016b, A&A, 593, A106
Saad S. M., et al., 2004, A&A, 419, 607
Saio H., et al., 2007, ApJ, 654, 544
Sampedro L., Dias W. S., Alfaro E. J., Monteiro H., Molino A., 2017, MNRAS, 470, 3937
Samus N. N., Kazarovets E. V., Durlevich O. V., Kireeva N. N., Pastukhova E. N., 2017, Astronomy Reports, 61, 80
Scargle J. D., 1982, ApJ, 263, 835
Semaan T., Hubert A. M., Zorec J., Gutiérrez-Soto J., Frémat Y., Martayan C., Fabregat J., Eggenberger P., 2018, A&A, 613, A70
Shokry A., et al., 2018, A&A, 609, A108
Sikora J., et al., 2019, MNRAS, 487, 4695
Silaj J., Landstreet J. D., 2014, A&A, 566, A132
Silva M. D. V., Napiwotzki R., 2011, MNRAS, 411, 2596
Skiff B. A., 2014, VizieR Online Data Catalog, 1, 2023
Slettebak A., 1979, Space Science Reviews, 23, 541

Smith M. A., Lopes de Oliveira R., Motch C., 2016, Advances in Space Research, 58, 782
Spear G. G., Mills J., Snedden S. A., 1981, PASP, 93, 460
Stefl S., Balona L. A., 1995, in Stobie R. S., Whitelock P. A., eds, Astronomical Society of the Pacific Conference Series Vol. 83, IAU Colloq. 155: Astrophysical Applications of Stellar Pulsation. p. 305
Tokovinin A., 2008, MNRAS, 389, 925
Townsend R. H. D., Owocki S. P., 2005, MNRAS, 357, 251
Townsend R. H. D., Owocki S. P., Howarth I. D., 2004, MNRAS, 350, 189
Tubbesing S., Rivinius T., Wolf B., Kaufer A., 2000, in Smith M. A., Henrichs H. F., Fabregat J., eds, Astronomical Society of the Pacific Conference Series Vol. 214, IAU Colloq. 175: The Be Phenomenon in Early-Type Stars. p. 232
Ud-Doula A., Owocki S. P., Townsend R. H. D., 2008, MNRAS, 385, 97
Ud-Doula A., Owocki S. P., Townsend R. H. D., 2009, MNRAS, 392, 1022
Walker G. A. H., et al., 2005, ApJ, 635, L77
Wang L., Gies D. R., Peters G. J., 2018, ApJ, 853, 156
Zorec J., Royer F., 2012, A&A, 537, A120
Zorec J., et al., 2016, A&A, 595, A132
ud-Doula A., Owocki S. P., 2002, ApJ, 576, 413
ud-Doula A., Owocki S. P., Kee N. D., 2018, MNRAS, 478, 3049

APPENDIX: NOTES ON ADDITIONAL STARS

In this section notes are given on stars not discussed in the main section. These stars were generally observed only in one sector. Periodograms are shown in Fig. A1. Where possible, the rotational frequency is estimated where a fundamental and its harmonic can be discerned in the periodogram. This might consist of a single peak and its harmonic, a broad peak and its harmonic or equally-spaced frequency groups each consisting of several peaks.

TIC 23037766, HR 2787. Balona et al. (1992) found possible light variations at 1.07 or 1.31 d^{-1} from ground-based photometry. The periodogram shows broad peaks at around 1.07 d^{-1} and its harmonic.

TIC 47296054, ϵ PsA. Balona et al. (2019) found a fundamental peak at 0.836 d^{-1}, assumed to be the rotational frequency, and three harmonics as well as an anomalous peak at 0.432 d^{-1} which is slightly different from half the fundamental frequency.

TIC 52665242, HR 2418. The fundamental peak at 1.145 d^{-1} and three harmonics are visible.

TIC 53992511, HR 8408. Cuypers et al. (1989) found a frequency of 2.53 d^{-1} or half this value from ground-based photometry. The periodogram shows multiple peaks indicative of an SPB pulsator. The lines sit on top of broad features which are repeated every 1.6 d^{-1}. This is taken to be the rotational frequency.

TIC 56179720, 56 Eri. From ground-based photometry, Balona et al. (1992) found multiple peaks at around 0.9 d^{-1}. Later, Stefl & Balona (1995) derived a single photometric frequency of 0.80 d^{-1}. The periodogram shows a close doublet at 0.66 and 0.80 d^{-1} and a stronger peak at roughly double the frequency, 1.44 $^{-1}$. We take this to be a possible SPB variable.

TIC 67251066, λ Cyg. This is a known multiple system (Tokovinin 2008). The periodogram shows two broad peaks at about 1.1 and 2.2 d^{-1} which is assumed to be due to rotation.

TIC 71132174, DU Eri, HR 1423. Balona et al. (1992) found a frequency of 0.82 d^{-1} and its harmonic. The periodogram shows multiple peaks in three frequency ranges, 1.2–1.6, 2.4–3.2 and around 4.0 d^{-1}. The time-frequency diagram appears to show frequency drifts, so we interpret these three frequency groups as due to rotation at about 1.4 d^{-1}.

TIC 71727949, HR 2142. This star is a Be+sdO binary system with an orbital period of 80.913 d (Peters et al. 2016). Barrera et al. (1991) found a frequency of 1.26 d^{-1} from ground-based photometry. The main feature in the periodogram is a broad peak at 2.265 d^{-1} which is variable in amplitude, but no rotational frequency can be determined.

TIC 75047606, HR 3670. There is very little light variation in this star except for a low-amplitude peak at 1.669 d^{-1} which we take to be the rotational frequency.

TIC 81584371, HR 2690, FV CMa. This is a close optical double with a brightness difference of 3.2 mag. Barrera et al. (1991) found a frequency of 1.92 d^{-1} from ground-based photometry. The periodogram is almost featureless apart from a low-amplitude broad peak at about 0.75 d^{-1} which is taken as the rotational frequency.

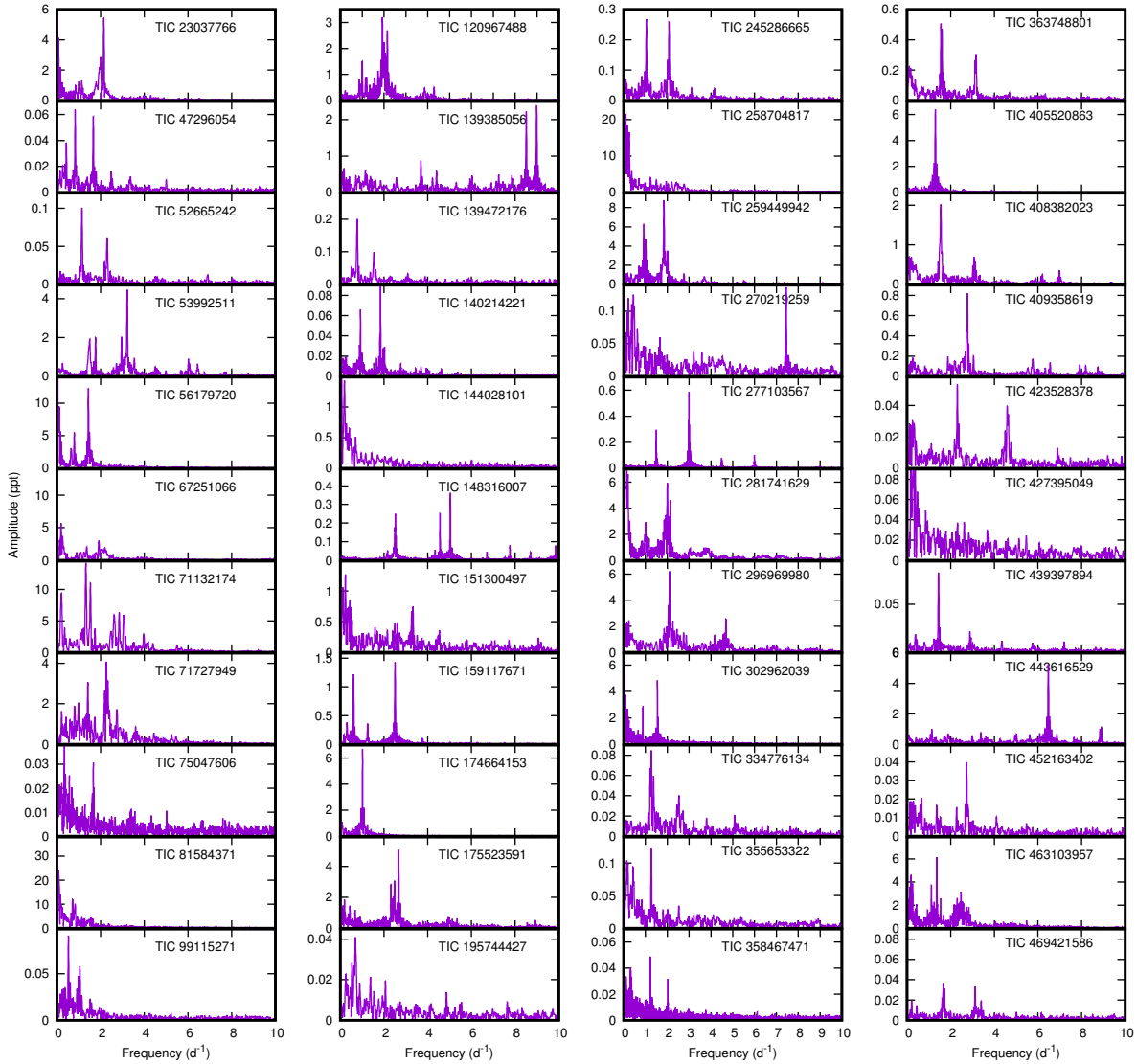

Figure A1. Periodograms of stars not discussed in the main section.

TIC 99115271, HR 7789. The periodogram shows a peak at 0.529 d^{-1}, which we assume is the rotational frequency, and its harmonic.

TIC 120967488, HR 7262. The periodogram shows three broad structures at frequencies 1.0, 2.0 and 4.0 d^{-1} which is assumed to be a result of rotation at a frequency of 1.0 d^{-1}.

TIC 139385056, HR 2855, FY CMa. The periodogram shows high frequencies typical of a β Cep pulsator, but no indication of a rotational peak. Table A1 lists the most significant extracted frequencies.

TIC 139472176, HIP 11116. The periodogram shows a single peak at 0.7727 d^{-1}, assumed to be rotation, and several harmonics.

TIC 140214221, HR 1956, α Col. A peak at 0.9258 d^{-1} and its harmonic is taken as rotation.

TIC 144028101, HR 5683, μ Lup. A low-amplitude peak at 33.156 d^{-1}, amplitude 0.16 ppt identifies this star as a Maia variable. No other significant frequency peak is present.

TIC 148316007, HR 2507. There is a large number of peaks in the range 2–20 d^{-1} indicating that this is a β Cep star (Table A1). A broad peak at 2.523 d^{-1} and its harmonic is taken to be the rotational frequency. The star lies somewhat below the zero-age main sequence.

TIC 151300497, HR 6397. This is a double-lined spectroscopic binary, with no significant variability.

TIC 159117671, HR 4893. The periodogram shows five peaks with frequencies which may be represented by a frequency 0.3058 d^{-1} and its harmonic and 1.2522 d^{-1} and its first two harmonics. The latter is assumed to be the rotational frequency. The lower frequency, which corresponds to a period of 3.27 d, may be of orbital nature. The star is in a multiple system with one of the components being a spectroscopic binary with a period of 3.2866 d (Tokovinin 2008).

TIC 174664153, HR 2968. This is a member of the open cluster NGC 2451B. The star appears to be a binary in an eccentric orbit with a period of 371 d (Carrier et al. 1999).

Table A1. Extracted frequencies, ν (d^{-1}), and amplitudes, A (ppt) for stars with high frequencies. The figures in brackets denote the error in the last digit.

ν	A	ν	A	ν	A
TIC 139385056.					
0.1727(6)	0.65(1)	6.0325(8)	0.45(1)	12.3253(9)	0.13(1)
1.1477(7)	0.53(1)	7.2484(7)	0.51(1)	12.6811(9)	0.09(1)
2.5689(8)	0.41(1)	7.8538(7)	0.49(1)	13.0979(9)	0.14(1)
3.6910(5)	0.86(1)	8.5140(2)	2.25(1)	13.3951(7)	0.54(1)
4.2221(8)	0.39(1)	8.9899(3)	2.40(1)	14.8955(9)	0.15(1)
4.4051(7)	0.59(1)	10.1424(9)	0.13(1)	15.1680(9)	0.09(1)
5.3059(9)	0.23(1)	10.8241(9)	0.31(1)	17.9759(9)	0.10(1)
5.9381(9)	0.35(1)	11.8906(9)	0.12(1)	22.3872(9)	0.09(1)
TIC 148316007.					
2.1640(4)	0.058(2)	7.7650(3)	0.082(2)	12.3314(9)	0.022(2)
2.5229(1)	0.238(2)	8.7062(5)	0.042(2)	13.2121(9)	0.021(2)
4.3382(5)	0.039(2)	9.8525(3)	0.081(2)	16.4693(9)	0.012(2)
4.5659(1)	0.242(2)	10.0119(1)	0.175(2)	16.5653(9)	0.013(2)
5.0403(1)	0.358(2)	10.8473(4)	0.050(2)	17.8625(9)	0.015(2)
6.7145(4)	0.045(2)	12.1613(4)	0.058(2)	18.5583(9)	0.015(2)
TIC 408382023.					
1.5481(2)	1.971(9)	5.8943(9)	0.155(5)	10.3183(9)	0.073(4)
3.0726(5)	0.653(7)	6.2010(7)	0.268(7)	13.9655(9)	0.114(5)
3.3370(9)	0.159(7)	6.9841(6)	0.358(7)		
TIC 409358619.					
1.8705(7)	0.193(5)	6.5570(9)	0.134(5)	11.5144(9)	0.106(5)
2.1763(9)	0.112(5)	7.9134(9)	0.119(5)	11.7959(9)	0.104(5)
2.3595(8)	0.152(5)	8.1915(9)	0.101(5)	12.3267(9)	0.118(5)
2.7678(2)	0.812(5)	8.7472(9)	0.087(5)	12.8563(9)	0.129(5)
3.0435(9)	0.134(5)	10.7575(9)	0.107(5)	14.7442(9)	0.091(5)
5.7636(7)	0.174(5)	10.9339(7)	0.191(5)		
TIC 443616529.					
1.1342(5)	1.03(1)	5.6259(8)	0.50(1)	8.8468(8)	0.78(1)
2.9881(8)	0.52(1)	6.0771(8)	0.67(1)	8.9063(5)	0.91(1)
3.3846(7)	0.74(1)	6.4739(2)	5.25(1)	12.1254(9)	0.18(1)
4.9365(8)	0.51(1)	6.8711(9)	0.41(1)	13.2080(9)	0.28(1)
5.0159(7)	0.53(1)	7.6464(9)	0.36(1)		

There is only one significant peak in the periodogram at $1.0185\,d^{-1}$ which we take to be rotation.

TIC 175523591, HR 3022. This star is classified as an eclipsing binary in the *General Catalogue of Variable Stars*, but no period is given. No eclipses are visible in the *TESS* data. The periodogram shows at least two groups at around $2.5\,d^{-1}$ and its harmonic. The first group comprises three distinct peaks at 2.674, 2.480 and $2.321\,d^{-1}$, but with amplitude variations, The mean frequency of about $2.5\,d^{-1}$ is taken as the rotational frequency.

TIC 195744427, HR 8028, ν Cyg. There are no distinctive features in the periodogram except a low-amplitude peak at about $0.69\,d^{-1}$.

TIC 245286665, HR 7719. The periodogram shows a presumed rotational frequency at $1.0393\,d^{-1}$ and three harmonics.

TIC 258704817, HR 5500. This is a double-line spectroscopic binary (Chini et al. 2012). The periodogram does not show any distinctive features.

TIC 259449942, HR 2921. This star, a member of the open cluster NGC 2422, contains a sdO companion in a long-period orbit (Wang et al. 2018). The periodogram shows a broad peak at $1.1\,d^{-1}$, assumed to be the rotational frequency, and several harmonics.

TIC 270219259, η PsA. The star is a close double with a brightness difference of 1.09 mag. Balona et al. (2019) found broad low-frequency features at around $1.7\,d^{-1}$ for part of the time. The most interesting feature in the periodogram is a sharp peak at $7.445\,d^{-1}$ (amplitude 0.139 ppt) which must be due to pulsation. We classify it as a Maia variable.

TIC 277103567, 29 Dor. From an analysis of ground-based and Hipparcos photometry, a very-low amplitude variation with a period of 395.48 d was determined. It was later confirmed from radial velocity measurements (Carrier et al. 2002). Balona et al. (2019) found a peak at $1.496\,d^{-1}$ and three harmonics. This is confirmed with the additional *TESS* data where a peak at $1.49668\,d^{-1}$, assumed to be the rotational frequency, and at least three harmonics are visible.

TIC 281741629, JL 212, BG Phe. This is a high Galactic latitude runaway Be star. No periodicity was found from the first two *TESS* sectors (Balona et al. 2019) and no further data are available. The possible subdwarf classification is due to Kilkenny & Muller (1989). The luminosity determined from the *Gaia* parallax places this star at the end of core hydrogen burning, so it cannot be a subdwarf.

TIC 296969980, θ Cir. This is a double-line spectroscopic binary (Chini et al. 2012) and an interferometric double with an orbital period of 39.61 yr (Mason et al. 2010). The periodogram consists of two peaks at 2.1047 and $4.6893\,d^{-1}$ on top of broad features. We classify it as SPB, No rotational frequency can be determined.

TIC 302962039, HR 3642. The periodogram features two sharp peaks at 1.5463 and $0.8875\,d^{-1}$. The light curve shows irregular variations with a timescale of about 40 d. No rotational frequency can be determined.

TIC 334776134, HR 4123. A broad peak at about $1.3\,d^{-1}$ and three harmonics are visible. We presume this to be rotation.

TIC 355653322, ϵ Tuc. Balona et al. (2019) found a low-amplitude peak at $1.2659\,d^{-1}$ and its harmonic. This is assumed to be the rotation frequency.

TIC 358467471, HIP 38779. This star is a member of NGC 2516. Two unrelated peaks are visible at $1.2278\,d^{-1}$ and $2.0282\,d^{-1}$. No rotation peak can be identified.

TIC 363748801, η1 TrA. The periodogram shows peaks at $1.5548\,d^{-1}$ (assumed to be the rotational frequency) and at least one harmonic.

TIC 405520863, 39 Cru, HR 4823. Balona et al. (1992) found a frequency of $1.295\,d^{-1}$ from ground-based photometry. The periodogram shows the same frequency, $1.2982\,d^{-1}$, which is assumed to be due to rotation. The 1st and 2nd harmonics are barely visible.

TIC 408382023, HR 3858. A broad peak at $1.55\,d^{-1}$, assumed to be the rotational frequency, and two harmonics are visible. In addition, some low-amplitude peaks between $5–13\,d^{-1}$ (Table A1) suggest that this is a Maia variable.

TIC 409358619, HR 5316. There are multiple peaks in the periodogram up to about $13\,d^{-1}$, indicating a β Cep star. Extracted frequencies are listed in Table A1. The first harmonic of the highest-amplitude peak at $2.7678\,d^{-1}$ is faintly visible. We assume this might be the rotational frequency.

TIC 423528378, ζ Crv, HR 4696. Barrera et al. (1991) found a photometric frequency of $1.96\,d^{-1}$. The periodogram shows a broad peak at $2.306\,d^{-1}$, assumed to be due to rotation, as well as the 1st and 2nd harmonics.

TIC 427395049, θ^2 Ori, HR 1897. This star is a double-line spectroscopic binary (O9.2V+B0.5V(n)) in a very rich field (Maíz Apellániz et al. 2019). No clear periodicity is visible in the periodogram.

TIC 439397894, 2 Cet, HR 9098. A peak at $1.4408\,\mathrm{d}^{-1}$, assumed to be the rotational frequency, and as many as 5 harmonics are visible. In addition, there is a much weaker peak at $0.357\,\mathrm{d}^{-1}$ and some harmonics which may perhaps be orbital in nature.

TIC 443616529, ϕ Leo. Evaporation of solid, comet-like bodies grazing or falling into the star has been proposed as the source of variable spectral lines (Eiroa et al. 2016). This is a δ Sct variable with several peaks (Table A1).

TIC 452163402, A Cen, HR 4460. The strongest peak in the periodogram is at $2.7323\,\mathrm{d}^{-1}$, but the sub-harmonic at $1.364\,\mathrm{d}^{-1}$ is present with a very low amplitude. This is assumed to be the rotational frequency.

TIC 463103957, HR 4009. A broad peak at $1.36\,\mathrm{d}^{-1}$ and its harmonic is taken as the rotation frequency.

TIC 469421586, HR 7843. This is a multiple system. A broad peak at $1.66\,\mathrm{d}^{-1}$ and its harmonic is taken as the rotational frequency. In addition, two peaks at 37.1229 and $41.574\,\mathrm{d}^{-1}$ (amplitudes 0.078 and 0.019 ppt respectively) suggest that it is a Maia variable.